Máster en Astrofísica

2022-2023

Spectro-Photometric Decompositions of BEARD Galaxies with MUSE

Javier del Socorro Prieto

Tutors: Jairo Méndez-Abreu & Adriana de Lorenzo-Cáceres
Universidad de La Laguna, 2023

Abstract

La existencia de grandes galaxias sin bulbo es un reto hoy en día para el modelo de cosmología actual, ΛCDM. Esta teoría afirma que las galaxias se forman de manera jerárquica, es decir, se forman primero las pequeñas y, por fusiones de estas, se forman las más grandes. Estas fusiones cambian la morfología de las galaxias, ayudando a crear bulbos clásicos, destruyendo los discos preexistentes y creando, en algunas ocasiones, otros discos mayores; por lo que no se entiende que una galaxia pueda crecer sin formar un bulbo. Este problema se acentúa por dos motivos: se encuentran más galaxias de las esperadas sin bulbo y la Vía Láctea es una de ellas, pues no tiene un bulbo clásico, solo una barra con un *boxy-peanut*. Para ello, el grupo BEARD seleccionó 66 galaxias de masa parecida a la Vía Láctea en el universo cercano, con la intención de encontrar los posibles caminos de formación de estas y poder explicar la existencia de nuestra propia galaxia. Este trabajo de fin de máster se encuadra dentro del proyecto BEARD, pues estudiaremos cuatro de esas 66 galaxias. Para este fin, BEARD aborda el problema desde cuatro puntos distintos, creando cuatro grupos de trabajo: de imagen de óptica profunda, de fotometría de banda estrecha, de espectroscopía de rendija larga y de espectroscopía de campo integral. Concretamente este trabajo se puede catalogar dentro del último de sus cuatro grupos, el de espectroscopía de campo integral. La principal diferencia es que este grupo trabaja hoy en día con datos de MEGARA y nosotros lo haremos con datos de MUSE con las ventajas que eso supone: mayor rango espectral para poder estudiar líneas de absorción importantes para el estudio de las poblaciones estelares y mayor campo de visión para el estudio de las zonas más externas de las galaxias. Además, este será el primer trabajo dentro de BEARD con un análisis de las poblaciones de los discos de las galaxias sin bulbo.

Para llevar a cabo este estudio realizaremos descomposiciones espectrofotométricas de los cubos de datos de nuestras cuatro galaxias: NGC1087, NGC4598, NGC5806 y NGC7448. Antes de realizar estas descomposiciones, debemos realizar un tratamiento previo: un *bineado* Voronoi de los datos para tener una buena señal a ruido utilizando el código VorBin y un análisis de la cinemática estelar con el código pPXF. Este código compara los espectros con varios modelos basados en la librería de MILES, ajustando la cinemática de la galaxia (v, σ, etc.) y dándole pesos a modelos con distintas edades y metalicidades hasta encontrar la combinación de estos que mejor se ajuste a nuestro espectro. Utilizando los resultados de cinemática podremos construir un cubo en reposo, corrigiendo los desplazamientos de los espectros hasta que en un mismo bin tengamos la misma longitud de onda en toda la imagen. Después sí, realizaremos las descomposiciones espectrofotométricas con C2D, un código muy novedoso en el estudio de morfología de galaxias (solo existen dos en el mundo). C2D hace uso del código GASP2D para realizar las descomposiciones fotométricas, el cual analiza el brillo superficial de una imagen bidimensional y lo divide en sus componentes morfológicas. C2D envía todas las imágenes en longitud de onda del cubo a GASP2D individualmente, recoge sus resultados y los junta en cubos nuevos. Finalmente, este código nos devolverá un cubo de datos por cada componente morfológica que ajustemos (bulbo, disco, barra), en los cuales haremos un análisis de poblaciones estelares pesadas en masa con pPXF. Además realizaremos también un análisis de las poblaciones en el cubo sin descomponer para poder ver las diferencias entre los resultados.

Una vez realicemos las descomposiciones y los análisis de poblaciones estelares encontraremos varios resultados interesantes. NGC1087 se trata de una galaxia solo disco (sin ningún tipo de bulbo) con poblaciones muy jóvenes y poco metálicas y con muchas regiones de formación estelar acentuadas por una fusión con otra galaxia reciente, la cual también ha creado un gradiente de metalicidades norte-sur. NGC4598 se trata de una galaxia barrada con diferentes estructuras como un cúmulo estelar joven y metálico como núcleo (y con una tendencia a poblaciones más jóvenes hacia el centro), un *boxy-peanut* en el centro de una barra también joven y metálica y un posible desierto de formación estelar en el disco, con una alta dispersión de poblaciones en esta región. NGC5806 se trata también de una galaxia barrada (aunque nosotros no hemos podido ajustar esta barra al ser más grande que el campo de visión), en cuyo centro se presenta un disco nuclear viejo y metálico rodeado de un anillo de formación estelar, el cual nos proporciona un gradiente suave de edades desde el centro hasta el anillo. En su disco, al analizarlo junto a la barra, encontramos poblaciones más viejas en el centro y una tendencia a poblaciones más jóvenes fuera. NGC7448 se trata también de una galaxia muy joven con mucha formación estelar y poco metálica con un pequeño bulbo con una edad algo mayor. Esta galaxia tiene tanta emisión de gas que tendremos que realizar un paso adicional previo a la descomposición, pues la emisión hace que el bulbo desaparezca en H_β. Por lo tanto tendremos que ajustar la emisión con pPXF y crear un cubo sin emisión.

Centrándonos principalmente en los bulbos y discos podremos observar varias cosas. Los bulbos son poco masivos en los tres casos en que tenemos un bulbo, y son metálicos. Encontraremos algo de dispersión en las edades, pues el disco nuclear de NGC5806 es un bulbo más viejo que los otros, pero si los comparamos con los datos de los bulbos extraídos con C2D en el proyecto CALIFA veremos que las desviaciones en edad y metalicidad están dentro de los valores típicos para los bulbos de este estudio. En cuanto a los discos, podremos afirmar que todos los discos observados son jóvenes, pues en ninguna región de ningún disco se había formado el 50% de la masa estelar hace 10 Gyr, mientras que se cree que en la Vía Láctea la mayoría de la masa estelar ya se había formado a esa edad. Incluso la mayoría de lar regiones de NGC1087 y NGC7448 no habían formado nada de masa hace 10 Gyr.

Contents

1. Introduction

1.1. Theorical background

The ΛCDM (Λ-Cold Dark Matter) model is a widely accepted cosmological model that describes the evolution and composition of the universe. According to this model, galaxies are embedded in a dark matter halo with a radius approximately 10 times the radius of luminous (baryonic) matter, based on radial density profiles (e.g. Navarro-Frenk-White, Navarro et al. [1996]). This model states that the universe is composed of 27% dark matter, 68% dark energy (Λ) and only 5% baryonic matter and it has an age of approximately 13.8 Gyr (Cimatti et al. [2019]).

The dark matter (DM) name refers to the fact that this matter is considered not to emit any electromagnetic radiation (such as light). In fact, it would not interact in any way with electromagnetic radiation, being completely transparent across the entire electromagnetic spectrum. This matter is found in the DM halos, which are formed by the growth of primordial perturbations in the matter density field in the early universe. These primordial perturbations can be measured, for example, in the Cosmic Microwave Background (CMB), which can be thought of as the remnants of the Big Bang thermal radiation. Such overdensities will continue to grow until they collapse gravitationally. These regions will consist mostly of DM but have a fraction of baryonic matter, which would form the primordial gas.

These initially small halos would eventually merge together. With each merger, the halo would grow larger and the amount of primordial gas would increase, until it reaches a point where the gas collapses, cools, and fragments, forming stars that give rise to a small galaxy. Larger galaxies would form later from more mergers. This is known as hierarchical galaxy formation, in which small galaxies and halos form first, and larger galaxies are created through mergers. These mergers between two smaller galaxies should result in the formation of new structures with new stellar populations, changing the morphology of the galaxy. For example, a merger can create a burst of star formation and the formation of an elliptical galaxy at the end. However, if the new galaxy still having remanent gas around from the merger, it might eventually fall back, creating a new disc structure with a bulge at the centre.

We need to understand the different types of galaxies depending on their morphology, so one of the ways to classify galaxies morphologically is visually by the Hubble sequence. This sequence is mainly divided into two types: early-type or elliptical (E) and late-type or spiral (S). Ellipticals are divided into 7 types depending on their apparent ellipticity, from spherical (E0) to the most elongated (E7). Spirals are divided into barred (SB) or not barred (SA), and are subdivided into 3 categories depending on the opening of the spiral arms and the prominence of the bulge (from less to more open, Sa, Sb and Sc). It also classifies lenticular galaxies (like spiral galaxies but without spiral arms) as S0. We can see this scheme in Figure 1. All this classification is explained in the book *"The Realm of Nebulae"*, Hubble [1936].

The main problem with this classification is that it is incomplete, so the De Vaucouleurs classification is more commonly used. This classification maintains the classification of spirals but adds

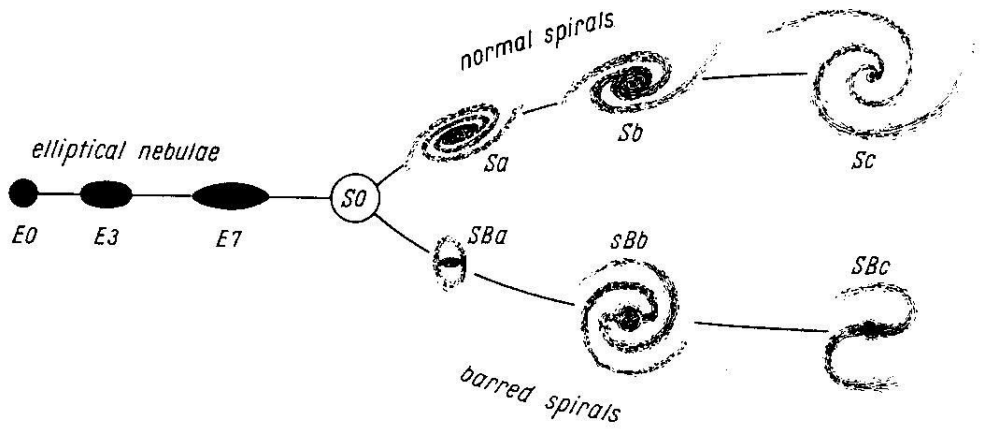

Figure 1: Sequence of Hubble's classification taken from the book *"The Realm of Nebulae"*, Hubble [1936]. In this figure we can see the different types of galaxies cataloged by Hubble according to their morphology.

irregular galaxies (Irr) and an intermediate type between spirals and irregulars (Sm). In addition, we can find galaxies with mixtures of morphological types, such as midpoints between barred (SB) and normal (SA) galaxies as SAB or mixtures between types a, b and c. He also introduced another subclassification according to the shape of their arms: if they are ring-shaped they will be denoted with an r in parentheses and if they are S-shaped with an s (we can also find mixed types, rs). We can see this scheme at Figure 2. All this classification is explained in de Vaucouleurs [1959].

The visual classification of galaxies is subjective and does not depend on physical properties. In addition, the shape of a galaxy can vary with inclination and wavelength. Still, it has its advantages, such as a trend of several important properties in figures 1 and 2: the further to the left we are in the Hubble or De Vaucoleurs outlines (early-type or elliptical) we will find pressure-dominated, non-star-forming, red-coloured galaxies with hot gas, while further to the right (late-type or spirals and irregulars) we will find rotation-dominated, star-forming, blue-coloured and cold-gas galaxies.

It is important to know the history of the mass that forms galaxies, where stars come from, and how they evolve in relation to their environment. Galaxies are complex systems, with distinct morphological regions formed by different stellar populations that affect each other in different ways. These regions can be affected by both external (such as mergers, gas inflows and outflows, etc.) and internal processes (death of stars what enrich the medium in metals, creating new, more metal-rich stars, AGNs, etc.). These processes that can destroy or create star formation zones are known as feedback. Knowing the different populations of the different morphological regions of the galaxy separately can be fundamental to understanding their history, to know how, when, and why stars were formed and to recreate their star formation history (SFH).

We only have information about a galaxy through the light it emits in our direction, by analysing its spectrum and his photometry. Therefore, if we want to study the populations of the different components of the galaxy separately, we must separate the light emitted by each component. To do this we make use of photometric decompositions (see subsection 3.3), an analysis of the surface brightness of the galaxy with different mathematical models. Nowadays, most photomet-

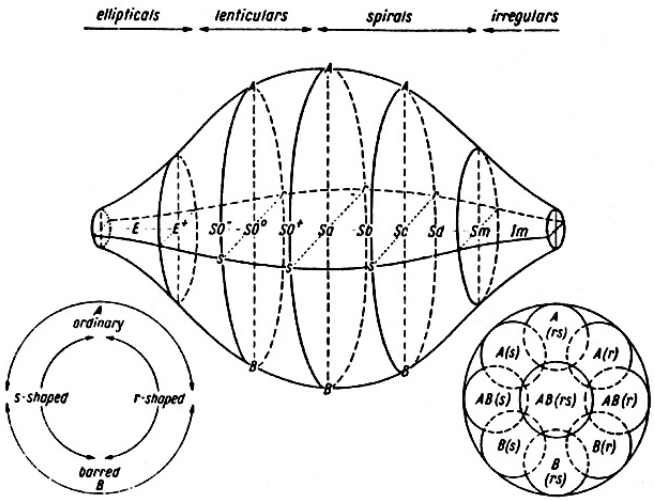

Figure 2: Sequence of De Vaucoleurs's classification taken from the book *"Classification and Morphology of External Galaxies"*, de Vaucouleurs [1959]. In this figure we can see the improvements made by De Vaucoleurs to the Hubble sequences, making a three-dimensional classification scheme.

ric decompositions are done in 2D, using a two-dimensional image of the galaxy. These codes combine different profiles taking into account the position angle of the components (to make the two-dimensional profile) and the fraction of light coming from each component. With they, we can create an individual image with the light coming from each component. There are several codes that perform these two-dimensional decompositions, for example GALFIT (Peng et al. [2002]), BUDDA (de Souza et al. [2004]), GASP2D (Méndez-Abreu et al. [2008]) or IMFIT (Erwin [2015]).

A further improvement to these codes is to add spectroscopic analysis to the photometric decomposition, creating a 3-dimensional decomposition. There are only two codes in the world that do this, BUDDI (Johnston et al. [2017]) and C2D (Méndez-Abreu et al. [2019]). In this work we will use C2D (see subsubsection 3.3.1), a code that uses GASP2D to perform the decomposition by adding the spectral information. This code is a tool unique in the world, so this analysis is something very new in the study of galactic morphology.

1.2. BEARD project

As we have seen in subsection 1.1, the largest galaxies are formed by a combination of mergers of galaxies according to the hierarchical formation, so galaxies with masses comparable with the Milky Way ($\log(M_\star/M_\odot) > 10.5$) should have suffered at least one major merger during their lifetime (we call major merger to all the mergers with a ratio of masses between both galaxies $m/M < 0.3$) (Stewart et al. [2009]). The problem is that many bulgeless galaxies with these masses have been observed in recent years. There are different definitions of what is a bulgeless galaxy, but the most common in the literature involves the fraction of light in the bulge (B/T), in particular $B/T < 0.1$ (Avila-Reese et al. [2014]). The fraction of bulgeless galaxies in the nearby universe is uncertain, but appears to be between 20% (Barazza et al. [2008]) and 74% (Kormendy et al. [2010]). This seems to contradict the ΛCDM model, so a more detailed study of

how these galaxies have formed could help us to understand galaxy formation better. Furthermore, the study of these galaxies is of vital importance, since the Milky Way is a bulgeless galaxy (Shen et al. [2010] suggested that, if the Milky Was has a bulge, it should have a brightness $B/D < 0.08$).

Therefore, massive bulgeless galaxies are still a challenge for ΛCDM models. A well characterised, volume-limited survey of giant bulgeless galaxies with the ability of tracing the merger history of these galaxies would be a terrific opportunity to test the hierarchical formation scenario versus this possible critical failure.

The BEARD project (Bulgeless Evolution And the Rise of Discs) was created with the intention of studying these bulgeless galaxies and trying to explain their structure and star formation history in the context of the ΛCDM paradigm. For this purpose, the collaboration selected a sample of 66 galaxies in which the following characteristics are fulfilled:

- Inclination: $i < 60°$, allowing a good photometric definition of the central region and limiting the dust effects.
- Concentration: $C = R_{90}/R_{50} > 2.5$, where R is the radius at which we would find a certain percentage of the galaxy's total light inside it, for example R_{50} would be the radius at which 50% of the light fits inside it. Graham and Driver [2005] suggested that a galaxy with this value of concentration can be considered as a late-type disc galaxy.
- Petrosian radius: $R < 10$ arcsec, to avoid small galaxies where we can found spatial resolution problems.
- Stellar mass: $\log(M_\star/M_\odot) > 10$, to have a sample of Milky Way-like galaxies.

BEARD project has as principal investigator Dr. Jairo Méndez-Abreu, along with a team of 25 other international researchers from different disciplines (stellar population, star formation, galaxy morphology and evolution, etc.) that combines observations and simulations, as well as with the help of master's and doctoral students. There are four main working groups depending on the type of observation:

1. Deep optical Imaging for the study of the low surface brightness stellar components in the outer regions of the galaxies. The Wide Field Camera (WFC) of the Isaac Newton Telescope (INT) will be used for this purpose.
2. Narrow-band photometry for the star formation rates that involves H_α and [NII] lines. For this, the IO:O instrument in the Liverpool telescope has been used.
3. Long-slit spectroscopy for stellar population gradients (age, metallicity and α/Fe). This were obtained with the instrument DOLORES in the Telescopio Nazionale Galileo (TNG).
4. Integral-field spectroscopy, to study the velocity dispersion of the nuclei of the sample galaxies, using the instrument MEGARA at the GTC.

There are no publications within this project yet, but there are several research projects within these four groups that are well advanced, so we will soon have quite a few publications from the BEARD project.

1.3. Objectives

This work could be classified in the last of the four groups in the BEARD project (see subsection 1.2), since we will use integral-field spectroscopy (IFS). But we will not use MEGARA, because we want the larger scale in both FOV and spectral range that MUSE provides. This spectrograph has not (yet) observed the BEARD sample galaxies for the BEARD project, but in the ESO science archive[1] we can find some datacubes of these galaxies observed for other projects with MUSE.

Therefore, this work will be the first within the context of the BEARD project that will work with MUSE data, involving several advantages such as a larger field of view that will allow us to perform integral-field spectroscopy on different components of the galaxy such as the disc and the bar (since MEGARA has a smaller FOV, only the bulge could be observed) and a larger spectral range that will allow us to analyse important lines (such as H_β, with importance for measuring the age of the stars, which is not observed with MEGARA, although there are already works to study this parameter without this line).

So, the objective of this work is to perform spectro-photometric decompositions of BEARD galaxies observed with MUSE. With this, we will be able to study the stellar populations of the different morphological components (such as bulge, disc and bar) separately, providing the first IFS study of discs in the BEARD project. By studying these populations we hope to shed light on how the different structures of bulgeless galaxies were formed, and to contribute to the search for the explanation of the existence of a large number of these galaxies.

[1] http://archive.eso.org/wdb/wdb/adp/phase3_spectral/form?collection_name=MUSE

2. Data

2.1. MUSE

In this TFM, we have analysed Multi Unit Spectroscopic Explorer (MUSE) data of four galaxies belonging to the BEARD sample. The data to be analysed are archival datacubes, which can be found on the website of the ESO science archive.

MUSE is an advanced instrument used at the Very Large Telescope (VLT) of the European Southern Observatory (ESO). It was installed in the Naysmyth-Focus B of Yepun, one of the four telescopes of the VLT located in the Paranal Observatory in Chile, and began operating in 2014. It belongs to the second generation of instruments of the ESO Paranal Observatory.

MUSE is an integral field spectrograph (IFS) that combines spectroscopic and imaging capabilities to obtain detailed data of astronomical objects. Using 24 Integral Field Units (IFU), MUSE obtains the spectra of the different areas of the observed field. The image is then reconstructed by creating a datacube, in which we have the astronomical object under study for each bin in wavelength. Therefore, we have an independent spectrum for each minimum spatial unit, which we will call spaxel (spectral pixel), in a single observation.

This instrument provides a very high spectral resolution, enabling the detection and analysis of spectral lines with great precision, covering a range from the ultraviolet to the near-infrared. Additionally, it offers significant spatial resolution, allowing for the investigation of internal structures within galaxies and other celestial objects in great detail.

MUSE has two main modes of observation: The Wide Field Mode (WFM) has a field of view (FOV) of 1×1 arcmin^2 with a spatial resolution around $\mathrm{FWHM} \sim 2.5$ px; and the Narrow Field Mode (NFM) that obtains a higher spatial resolution using a lower FOV. The data cubes used in this work have been obtained with the WFM, which obtains a larger field and uses a shorter integration time. This mode used (WFM) has a pixel spatial size of 0.2x0.2 arcsec^2 and a spectral bin of 1.25 Å px^{-1}, with a range of 4750-9350 Å and a spectral resolution about $R \sim 3000$. All this information about MUSE has been obtained from the MUSE user manual, developed by Richard et al. [2021].

2.2. BEARD Galaxies

Our sample is composed of the following four Milky Way-like galaxies: NGC1087, NGC4598, NGC5806 and NGC7448. Their coordinates, redshift and galactic morphology have been obtained from NED database[2].

NGC1087 is a spiral galaxy of type SAB(rs)cs, with an apparent magnitude of 12.2. It was discovered in 1785 by William Herschel. Its coordinates are 2h, 46m 25.2s right ascension and -0°

[2] http://ned.ipac.caltech.edu/

29′ 55″ declination, with a central redshift of 0.00508. It was observed by MUSE on November 13, 2017. The data cube consists of a mosaic of 6 images from 4 exposures each one and belongs to the PHANGS-MUSE survey (Emsellem, Eric et al. [2022]). The programme ID is 1100.B-0651(a) with principal inverstigator (PI) Eva Schinnerer. In the BEARD project (in a paper in preparation) they have observed that this galaxy has a tidal arm in its southern part, a "tail" above a galaxy of gas and stars. This seems to indicate that this galaxy has recently undergone a merger or is even undergoing one at the moment (but there is no remaining trace of the companion galaxy).

NGC4598 is a barred lenticular galaxy (SB0 type) discovered by William Herschel in 1784. It has an apparent magnitude of 13.6 and its coordinates are 12h, 40m 11.9s right ascension and 8° 23′ 0.1″ declination, with a central redshift of 0.006541. It was observed by MUSE on February 13, 2021. The data cube consists of a combination of 13 exposures and the programme ID is 0106.B-0158(A) with PI Virginia Cuomo.

NGC5806 is a spiral galaxy of type SAB(s)b, with an apparent magnitude of 12.2. It was discovered by John Herschel in 1786 and has the particularity that in recent years many supernovae have been reported in it. Its coordinates are 15h, 00m 00.4s right ascension and 1° 53′ 28.7″ declination, with a central redshift of 0.0045. It was observed by MUSE on April 7, 2016. The data cube consists of a combination of 4 exposures. The programme ID is 097.B-0165(A) with PI Marcello Carollo.

Finally, NGC7448 is a spiral galaxy of type SA(rs)bc, with an apparent magnitude of 11.4. It was discovered by William Herschel in 1784. Its coordinates are 23h, 00m 03.6s right ascension and 15° 58′ 49″ declination, with a central redshift of 0.00732, which makes it the farthest galaxy in our sample. It was observed by MUSE on June 23, 2018. The data cube consists of a mosaic with two single exposure images. The programme ID is 0101.B-0706(A) with PI Jesse Van de Sande.

3. Methodology

The objective of this work is to perform spectro-photometric decompositions of four galaxies which take part of BEARD sample and that have been observed with MUSE. For this purpose we will use the C2D code (Méndez-Abreu et al. [2019]). C2D makes use of the GASP2D code, which performs the photometric decomposition of a two-dimensional image.

To perform the spectro-photometric decomposition with C2D, we have to make first a data processing, which includes binning the data (to increase the S/N of individual spaxels) and the correction of the stellar kinematics, in order to create a restframe datacube for each galaxy. After performing the spectro-photometric decomposition, we will use the pPXF code to carry out an analysis of the stellar populations of each structural component.

3.1. Voronoi binning

When we want to analyse spatially resolved astronomical data, it is common to find pixels (or spaxels) in which the noise is so high that we cannot obtain physical solutions from their analysis. We must try to improve the signal over the noise, in other words, to improve the S/N. For this purpose, binning is often used. As the noise grows with the root of the signal, binning various spaxels together will improve the S/N. That also implies that we will lose spatial resolution, but the information obtained will be of much better quality.

The binning method used in this work will be Voronoi binning. This technique analyses each spaxel and, if the S/N of that spaxel does not reach a previously chosen minimum, it will join it with other contiguous spaxels until they reach the indicated S/N value. With this method, the binning starts at the centre of the galaxy (spaxel with the best S/N) and measures the S/N of each spaxel in a spiral towards the outermost parts of the galaxy. This form of binning ensures that we do not lose the spatial information of areas with acceptable S/N (e.g. galactic centres). Once the binning is applied, each minimum region of spatial information (each spaxel junction or spaxel that was left alone because of sufficient S/N) will be called a voxel. Further information on the Voronoi binning method can be found at Cappellari and Copin [2003].

The code used for this binning is called VorBin, a code written in Python and developed by M. Capellari. An example to the code can be found at his website[3]. To begin with, we integrate a stellar continuum region (5400-5700 Årange), over which we will calculate the Voronoi. We remove the spaxels with S/N < 3 from our integrated star continuum images. This is because we are going to apply a Voronoi binning with S/N $\sim$ 20 and many of these spaxels would mostly add more noise and no much information, altering our final results. The code then starts the iteration with the spaxel with the best S/N, and continues sweeping the surroundings in a spiral. Finally, the code returns a map with the spaxels that it has joined together to reach the set value of S/N (in our case, 20). We will have to apply this map to each bin in wavelength of our cubes, gathering the signals of the spaxels that belong to the same voxel (averaging them). With this, we would already

[3] https://www-astro.physics.ox.ac.uk/~cappellari/software/

have our datacube with the required S/N for a physical analysis.

3.2. Stellar Kinematics

Galaxies are systems in motion. By galaxy kinematics we mean the measure of the motion of the matter that makes up a galaxy. This does not only refer to stars, as gas and dust also have kinematics and do not necessarily have to be the same as stars. The velocity is a vector, so it can be decomposed into three axes. Because of the great distance separating us from these galaxies and because the human time scale is tiny compared to galactic time scales, we can only measure one component of this velocity, the transverse, line-of-sight velocity.

Due to the different velocities in the different regions of the galaxy, the spectra emitted by each of these regions will move in wavelength by a different amount due to the Doppler effect,

$$v/c = \frac{\lambda_{\rm obs} - \lambda_{\rm rf}}{\lambda_{\rm rf}} = \frac{\lambda_{\rm obs}}{\lambda_{\rm rf}} - 1, \tag{1}$$

where v is the line-of-sight velocity at which that region is moving, c the speed of light, $\lambda_{\rm obs}$ the wavelength at which line was observed and $\lambda_{\rm rf}$ the wavelength at which it was emitted. By measuring, for example, emission or absorption lines at a given wavelength and knowing at what wavelength that phenomenon occurs at rest, we can calculate the line-of-sight velocity.

It should be mentioned that the shift of the lines in the spectrum is not only the rotational velocity of a given region of the galaxy, there are other extra velocities that affect the whole galaxy equally, systematic velocities such as the rotational velocity of the Earth, our velocity relative to the Sun, the velocity of the Sun relative to the centre of the Milky Way or the redshift that the whole spectrum of the galaxy undergoes due to the expansion of the universe. The last one should not be treated as a velocity, because the galaxy is not moving away from us, but it is the space that is expanding as the light moves towards us, shifting the spectra, so we should resort to cosmological scaling factors. Our sample consists of very close galaxies, for which this line shift can be treated as another Doppler effect (Equation 1). For this it has to be satisfied that their "velocity" caused by the expansion of the universe is $v \ll c$ (the greater the distance, the greater the shift and therefore this approximation is no longer valid for more distant galaxies). This redshift will be the one that affects the spectrum the most. All these systematic velocities are included in the cosmological redshift, $z \simeq v_{\rm sys}/c$, and affect the whole galaxy equally, so the alterations to this redshift in each different region will be given by the rotation of the galaxy.

If we want to "correct" the spectra measured for a given galaxy we will have to move the wavelengths towards blue according to their velocity, but if we do this movement on a linear scale we will have to shift a different amount for each wavelength, because we have to move the spectrum by an amount of $\Delta\lambda$, and making use of Equation 1 we get that

$$\Delta\lambda = \lambda_{\rm obs} - \lambda_{\rm rf} = \lambda_{\rm rf}\left(1 + \frac{v}{c}\right) \sim \lambda_{\rm rf}, \tag{2}$$

in other words, each wavelength shift depends on its own wavelength value. On the other hand, by using the logarithm of the wavelength, the amount we need to shift will be constant across the entire spectrum and only depend on the velocity of the region in question,

$$\Delta \ln \lambda = \ln \lambda_{\rm obs} - \ln \lambda_{\rm rf} = \ln \left(1 + \frac{v}{c}\right) \sim \frac{v}{c}. \tag{3}$$

Another important concept in galactic kinematics is the velocity dispersion σ, which we can interpret as the Full Width at Half Maximum (FWHM) of the lines, corrected by instrumental dispersion,

$$\sigma = \frac{c}{\lambda_{\rm rf}} \frac{\sqrt{\mathrm{FWHM}^2_{\rm obs} - \mathrm{FWHM}^2_{\rm inst}}}{2.355}. \tag{4}$$

This parameter is important because a low stellar velocity dispersion means that all the stars in the region are moving in a very similar way, which usually indicates a general and joint rotation of the stars (for example a disc), while higher values indicates more independent motion of the stars, as occurs in bulges or elliptical galaxies. Therefore, a good analysis of this parameter could help us determine the morphology of the galaxy.

The line-of-sight velocity and the velocity dispersion are, respectively, the first two moments of the line-of-sight velocity distribution (LOSVD), which is a statistical measure of the distribution of velocities of stars or objects in a galaxy along the line of sight. LOSVD describes how the velocity varies along the line of sight, providing valuable information about the internal dynamics of the galaxy. This term can be parameterized (that is why we talk about velocity and dispersion as its first two moments), and can have higher moments that will indicate different properties (e.g. h_3 indicates tangential anisotropy, h_4 radial anisotropy, etc.), but for the study of this work we will focus only on the first two moments.

3.2.1. pPXF code for kinematics

As we describe in the subsection 2.1, MUSE has a high spectral and spatial resolution, and our BEARD galaxies are rotating discs, so we will have in the same quasi-monochromotic bin different wavelength values in each voxel. Then, to perform the spectro-photometric decomposition, we need to have the same wavelength for all the voxels throughout the galaxy in each wavelength bin. To determine the kinematics of the galaxies, we will use pPXF (Cappellari and Emsellem [2004]).

pPXF (Penalized Pixel-Fitting) is an algorithm wrote in Python used to fit observed spectra to a linear combination of model spectra, with the aim of obtaining information about the physical properties of the observed sources, such as stellar velocities and the relative contribution of different stellar or gaseous components. This code was developed by M. Capellari and an extensive explanation can be found in Cappellari [2022].

The code uses a nonlinear fitting approach based on the least-squares technique. It fits the observed spectra with a linear combination of the selected spectral models. The algorithm searches for the optimal weights assigned to the models to minimize the differences between the observed spectra and the models. Then, employs penalization and regularization techniques to control the fitting and prevent non-physical or unstable solutions. These techniques help avoid overfitting and ensure a smooth and realistic solution.

For the comparison we need a set of spectral model that will be used for the fitting. In our case we will use the MILES-based models[4], a combination of SSP with different ages and metallicities. These models have been built on the basis of the MILES (Medium-resolution INT Library of Empirical Spectra) star library, from spectroscopic observations of several taken with the Isaac Newton Telescope. For this work we will use the UV-extended E-MILES stellar population models, explained at Vazdekis et al. [2016].

These models are Single Stellar Population (SSP), the spectrum that would make up an infinitesimal burst of star formation (all stars of the same age and metallicity). These SSPs are constructed using an IMF (Initial Mass Function, a statistical function that tells us how many stars would be created for each stellar mass value), isochrones (the paths that stars of each mass would follow in the HR diagram over their lifetime) and a library of stellar spectra for comparison. Specifically, the models used use the Kroupa IMF (Kroupa [2001]) and BaSTI isochrones (Pietrinferni et al. [2006]), and are based on the MILES libraries, as mentioned above. We will use a total of 315 SSPs with ages between 0.007 and 14 Gyr and metallicities between -1.26 and 0.26.

We will not need the full spectrum offered by MUSE, so we will reduce the fit to a range of 4700-5600 Å. In order to fit the stellar kinematics we will re-scale our spectrum by a multiplicative polynomial of order 6. We chose this order (and not a higher one that would better fit the spectrum) because right now we only want to fit the kinematics, knowing how much the lines have moved in the spectrum, we are not going to calculate properties that involve knowing the depths of these lines. We can choose the number of moments of the LOSVD to fit, and we will fit two: velocity v and velocity dispersion σ. Moreover, as we do not care about other physical properties right now, we will not use regularisation (which will reduce the computation time) and we could even mask the emission lines (although we have chosen to fit the gas as well, in order to have its kinematics).

Using the best fit associated to each voxel we move the spectrum in wavelength, depending on its stellar velocity (in a logarithmic scale of lambda, Equation 3). In order to reconstruct each bin with all voxels at the same wavelength value, we will have to do an interpolation of each spectrum and choose the flux for the wavelength that the spatial bin will have (since, by moving the spectra of each voxel independently, each spatial bin of each voxel will have a different lambda from the other voxels). Putting these spectra together with their corrected kinematics, we build a restframe datacube, i.e. a cube where the entire image of each wavelength bin is at the same wavelength. Now we can now perform the spectro-photometric decomposition.

[4] http://miles.iac.es/

3.3. Photometric decompositions

As we have seen in subsection 1.1, a galaxy has different morphological components such as discs, bulges and bars, and each will have independent stellar populations that emit light independently of the others. All of this light reaches us together, but we can separate it using photometric decompositions. This consists of using a number of parametric profiles to describe the surface brightness distribution of the different structures in the galaxy.

The profile used to describe elliptical (bulge-like) components or elliptical galaxies is the Sérsic profile (Sérsic [1963]). We can express this profile as

$$I_{\rm b}(r) = I_{\rm e} \exp\left\{ -b_n \left[\left(\frac{r}{r_{\rm e}} \right)^{1/n} - 1 \right] \right\}, \tag{5}$$

where $r_{\rm e}$ is the effective radius, $I_{\rm e}$ is the effective surface brightness (brightness at $r_{\rm e}$), n is the Sérsic index (for $n = 4$ we would have a Vaucouleurs profile and with $n = 1$ we would have an exponential profile) and b_n is the function that ensures that $r_{\rm e}$ contains half of the light, which we can approximate to $b_n = 2n - 0.327$ for $0.5 < n < 10$ (Capaccioli [1989]).

An exponential profile (Freeman [1970]) is often used to describe discs, which we retrieve from Equation 5 by making $n = 1$,

$$I_{\rm d}(r) = I_0 \exp\left(-r/h\right), \tag{6}$$

where I_0 is the central intensity and h is the disc scale length, which we can determine as the galactic radius at which the intensity decreases by a factor e^1.

The single exponential profile (Equation 6) can often describe the surface brightness profile of a galaxy (Type I disc), but many of these discs are best described by a double exponential law, changing the slope of the profile at a certain point ($r_{\rm break}$), and may be down-bending (Type II) or up-bending (Type III) on the outside. One way to describe these discs is with the truncated exponential profile (Méndez-Abreu et al. [2017]),

$$I_{\rm d}(r) = I_0 \left[\mathrm{e}^{\frac{-r}{h_{\rm in}}} \theta + \mathrm{e}^{\frac{-r_{\rm break}(h_{\rm out}-h_{\rm in})}{h_{\rm out} h_{\rm in}}} \mathrm{e}^{\frac{-r}{h_{\rm out}}} (1-\theta) \right], \tag{7}$$

where

$$\theta = \begin{cases} 0 & if \quad r > r_{\rm break} \\ 1 & if \quad r < r_{\rm break}. \end{cases}$$

As we can see, for different values of θ, we recover the exponential profile (Equation 6) with different values of h.

Finally, to describe a bar we use the Ferrers profile (Ferrers [1877]), which describes the surface brightness as

$$I_{\rm bar}(r) = I_{0,\rm bar}\left[1-\left(\frac{r}{a_{\rm bar}}\right)^2\right]^{n_{\rm bar}+0.5} \qquad \text{for} \quad r \leq a_{\rm bar}, \tag{8}$$

where $I_{0,\rm bar}$ is the central surface brightness, $a_{\rm bar}$ the lenght of the bar and $n_{\rm bar}$ the shape parameter. For a bar we use $n_{\rm bar} = 2$ (Laurikainen et al. [2005]). The sum of the surface brightness distributions of the different profiles will create a model of the brightness of the galaxy under study.

3.3.1. Spectro-photometric decompositions: C2D

To perform our spectro-photometric decomposition, we will use C2D, a code written in IDL by Jairo Méndez-Abreu, Sebastián Sánchez and Adriana de Lorenzo-Cácecres. As mentioned above, C2D is a unique code which performs a spectro-photometric decomposition of the different components of a datacube (there are only two such codes in the world). It makes use of the GASP2D code, which performs photometric decompositions of two-dimensional images. C2D sends each wavelength bin to GASP2D, which performs the wavelength-by-wavelength decomposition independently. As a result, we have the spectral and spatial information of each component included in the fit (Méndez-Abreu et al. [2019]). Morphologically, we can decompose a galaxy into its structural components (bulges, discs, bars) with independent surface brightness profiles (Equation 5 to 8). C2D allows us to choose which of these structural components we want to adjust to our galaxy.

The photometric decomposition of each bin (independent of the wavelength) is performing by GASP2D (Méndez-Abreu et al. [2008]). This code separates the light in our two-dimensional image of the galaxy according to which structural component it comes from (following the profiles described for each component, Equation 5 to 8), creating a new image with only the light from each component. As a two-dimensional decomposition, it takes into account the ellipticity and position angle of the different structures shaping a galaxy. In order to perform this decomposition, we must give an initial value to each parameter of the profiles (as well as to the ellipticity, position angle and fraction of light coming from each component) with which it will start the iterations until the best fit is found.

To begin with, we have to choose the initial conditions for each free parameter of the profiles. We have to be precise when we choose the initial conditions to avoid possible errors when running the code, so we will choose as initial conditions the values obtained in the decomposition with SDSS images of our galaxies by another work within the BEARD project, S. Zarattini et al [in preparation] (see Table 1). When running C2D we will find small variations in the values of these parameters for different wavelengths, but always with values very close to the chosen ones. Once we have chosen our initial values, C2D collapses the whole spectral range into 10 spectral bins and runs GASP2D on each of these integrated images like if they were independent images. For these fits we leave all the parameters of the profiles free, in order to find the best fit of the profiles to each bin. Then, with these 10 best values covering differents wavelengths for each parameter, we will make a linear fit of each of those parameter in order to assign a value to each wavelength across the entire spectral range. The code then calls GASP2D again, this time to fit each wave-

Table 1: Initial condition used in C2D. These values are those obtained by photometric decomposition of the SDSS images of BEARD galaxies by S. Zarattini et al. [in preparation].

	Galaxy	NGC1087	NGC4598	NGC5806	NGC7448
Bulge	$r_{\rm e}$ **(arcsec)**	1.74	1.19	4.09	2.00
	n	1.08	1.15	1.57	0.78
	$(b/a)_{\rm bulge}$	1.00	1.00	0.64	0.69
	$PA_{\rm bulge}$ **(degrees)**	176.08	45.49	162.97	172.62
Disc	$h_{\rm in}$ **(arcsec)**	29.13	15.86	22.25	36.31
	$(b/a)_{\rm disc}$	0.69	0.79	0.55	0.49
	$PA_{\rm disc}$ **(degrees)**	1.72	110.16	166.00	170.52
Bar	$a_{\rm bar}$ **(arcsec)**	-	23.76	-	-
	$n_{\rm bar}$	-	2.00	-	-
	$(b/a)_{\rm bar}$	-	0.37	-	-
	$PA_{\rm bar}$ **(degrees)**	-	161.24	-	-

length of the original datacube by fixing the structure parameter values that the linear fit gives for each wavelength (except for the effective intensities of the diferent components, which are left free).

It is important to say that NGC5806 has a bar (with $b/a = 0.32$), but this has a much larger radius than the observed FOV of MUSE, so we cannot adjust it. Therefore, in our decomposition we find the stars of the bar that will be associated in the disc datacube. S. Zarattiniet al. [in preparation] make the decomposition of this galaxy with and without bar, so we use the result of the fitting without bar. In addition, NGC4598, NGC5806 and NGC7448 have a truncated disc profile, but this also lies outside the FOV, so it does not affect our results.

Once all the fits of all the wavelength bins have been completed, C2D returns various cubes by putting together all the individual results for each wavelength obtained directly from GASP2D:

- A datacube for each selected component (bulge, disc, bar) with the models of this component for each wavelength bin.
- A datacube with the total model: a sum of all the models of the different components.
- A datacube for each component that we create using their relative light contribution multiplied by the rest-frame galaxy datacube. We derive for each wavelength the relative light contribution of each component model to the total model for each spatial voxel. Then, wavelength-by-wavelength, we multiply this fraction of light of each voxel (B/T , D/T , Bar/T) by the value of the same voxel in the galaxy restframe datacube, building a new datacube for each component. This will be the datacubes of the component in which we will analyse the stellar populations.
- The cube with the residuals (the difference between the total model and the restframe datacube for each wavelength bin).

This code was originally written to work with CALIFA data, so we had to rewrite it to work with our MUSE data, in particular because of the differences in spatial and spectral resolution.

It should be noted that with NGC7448 we had to re-treat the datacube before using C2D to remove the gas emission. This is due to the high emission in lines such as H_β, in which the bulge seemed to disappear in the image, causing C2D to return a value of 0 around that wavelength range for the bulge datacube.

3.4. Stellar Populations: pPXF

Once we have the spectro-photometric decompositions done and we have a datacube of each morphological component, we can analyse the stellar populations of each component separately. For this purpose we will use the pPXF code again, which we have already explained in the subsubsection 3.2.1, but with some differences.

Now, we use a multiplicative polynomial of order 8 in this fit (again, only in the range of 4700-5600 Å). In addition, we want to get more physical results, so it will be necessary to use regularisation. This parameter will increase the computation time considerably, but now we want to recover the weights of each SSP model with a higher accuracy (in subsubsection 3.2.1, we did not care about the combination of SSP for each fitting, only about how much the lines had moved). As we have a long spectrum, we will use a factor 100 of regularisation. Furthermore, we fix the kinematic values obtained in subsubsection 3.2.1 (σ and $v = 0$, as we have set the spectrum in restframe), due to the existence of a degeneracy between metallicity and velocity dispersion (Z-σ), because both properties affect the width of the lines. Finally, we must now fit the gas (although we also did this before), because masking these emission lines would remove important information in the absorption lines, such as H_β, which we need to find the age of the stars in a given voxel.

To compare our fit we will again use the MILES models. This comparison provides us several information, like age and metallicity of each voxel. It is important to notice that these models are normalised to one solar mass unit, i.e. the flux of each spectrum is normalised to a unit of solar mass. This normalisation makes the ages and metallicities results mass-weighted.

pPXF give us the age of the stars in each voxel in Gyr, and when we talk about metallicities of stars we will talk about abundances of certain elements. Specifically, pPXF uses the abundance $[M/H]$. M refers to elements heavier than hydrogen, so it is the abundance of these elements relative to the abundance of hydrogen. This measure is made in logarithm and is given as a function of this abundance in the Sun,

$$[M/H] = \log\left(\frac{M}{H}\right) - \log\left(\frac{M}{H}\right)_\odot . \tag{9}$$

As we have said, we will perform this analysis with each datacube of each component, but we will also add another analysis of the restframe datacube of the whole galaxy, in order to compare the results of each component with those obtained for the whole galaxy.

4. Results and discussion

Now, we will analyse the results obtained by following the steps described in section 3. We will first analyse the results obtained from the stellar kinematic analysis of the four galaxies, comparing them with each other. Then we will move on to a galaxy-by-galaxy analysis. We can look at the voxel-by-voxel analysis of stellar populations for each morphological component, deriving the possible star formation pathways for each galaxy, and comparing with previous work in our discussion. Finally, we will compare the age and metallicity of the bulges of our galaxies with those of the CALIFA survey (Méndez-Abreu et al. [2021]) to determine whether bulgeless galaxies occupy a special place among the rest of the galaxies.

4.1. Kinematics

First, we start with the stellar kinematics obtained with pPXF for each voxel. As we can see in the Figure 3, our four galaxies are rotating discs with a range of maximum velocities of 70-150 km/s. The velocity dispersions are generally very low ($\sim$ 40-100 km/s), indicating the predominance of the disc in the 4 galaxies, as expected. NGC1087, NGC5806 and NGC7448 have a rotation that appears to be flat, varying its velocity on the two axes (although for NGC5806 it would be flat with a velocity peak), while the rotation of NGC4598 looks more like that of a solid body, which only varies the velocity on a single axis (as well as being the galaxy with the lowest velocity dispersions and the lowest velocity values too).

We do not see any central component that could indicate a major bulge in our sample of galaxies, excepyt for NGC5806, in which we can observe a corotating velocity component and a central area of higher dispersion surrounded by a low-dispersion. This central structure closely resembles the nuclear disc and ring structure described by Bittner et al. [2020]. They suggest that the rings surrounding these nuclear discs are (often) a frontier region of star formation that is causing this nuclear disc to grow. They find that these nuclear discs have high velocity and velocity dispersion but that the star formation rings have lower velocity dispersion than their surroundings, as is the case for NGC5806. In subsection 4.4 we will check whether their trends in ages and metallicities are also in line with those obtained by this study.

4.2. NGC1087

Now, we will start with the analysis of the spectro-photometric decompositions and the stellar populations of our galaxies. The first galaxy to be studied is NGC1087. In the spectro-photometric decompositions we fit a bulge-disc galaxy (see Table 1). Integrating the whole MUSE spectral range given for each component we obtain a fraction of light in the bulge $B/T = 0.022$, in the disc $D/T = 0.978$ and compared $B/D = 0.022$, values that are in line with what is expected for a bulgeless galaxy.

Now, we can analyse its mass-weighted stellar population maps obtained with pPXF (see Figure 4). We see that this galaxy consists of an extensive young disc with several low-metallicity

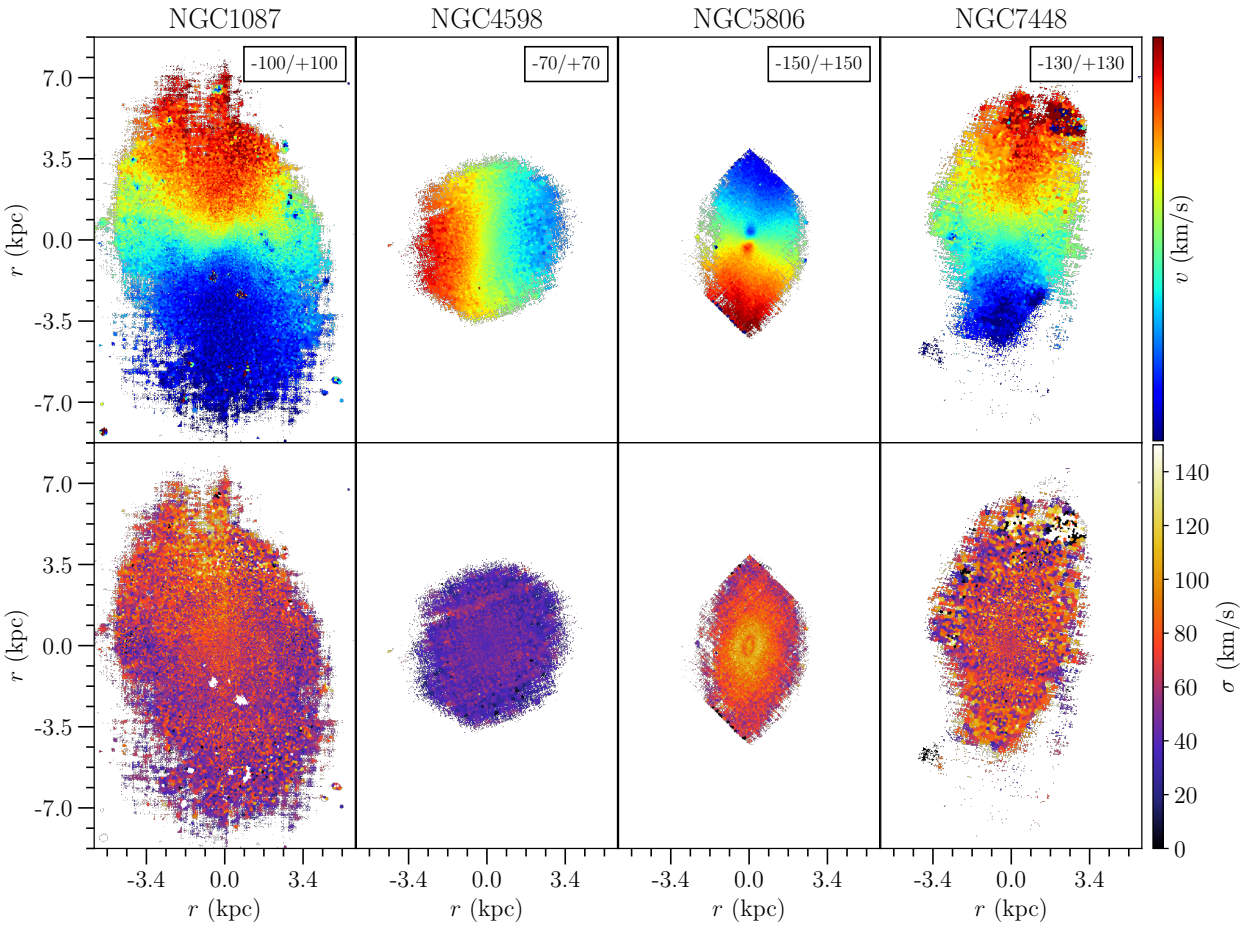

Figure 3: Stellar kinematics maps, plotting the two first moments of LOSVD, velocity (up) and velocity dispersion (down). From left to right we have NGC1087, NGC4598, NGC5806 and NGC7448. In each velocity map (up) the green colour corresponds to the systematic velocity of the galaxy and we have the maximum and minimum velocity (with respect to their systematic velocities) in the top right-hand corner of each map. All galaxies are scaled by their radii in kpc.

star-forming bursts (small regions with very low age and metallicity, mostly in the upper part of the galaxy) and a gradient of metallicities in its disc from up (less metal-rich) to down (more metal-rich). We also see a concentration of older populations towards the centre (although not even 3 Gyr old), but separated by four bursts of star formation in a row right in the centre. A little further south we see two older regions. In general we find low metallicities, except for a cone in the lower right centre, which reaches high metallicities. These features can be explained by the fact that, as we say in subsection 2.2, NGC1087 is undergoing a merger on its southern side (hence the gradient of metallicities from north to south), which will be triggering star formation in the galaxy and forming a very young disc.

Another thing to note is that its supposed bulge is another of these low-metallicity star-forming bursts (we also find 4 in a row in the central zone), with no difference between any of them. This region has a lot of gas emission which indicates star formation (see Figure A.1), so we could affirm that this central region is not a bulge, only a star-forming region that has been located in the centre of the galaxy. From now on we will treat this galaxy as a pure disc galaxy with $B/T = 0$.

For all our galaxies we will analyse the radial behaviour of their age and metallicity (mass-

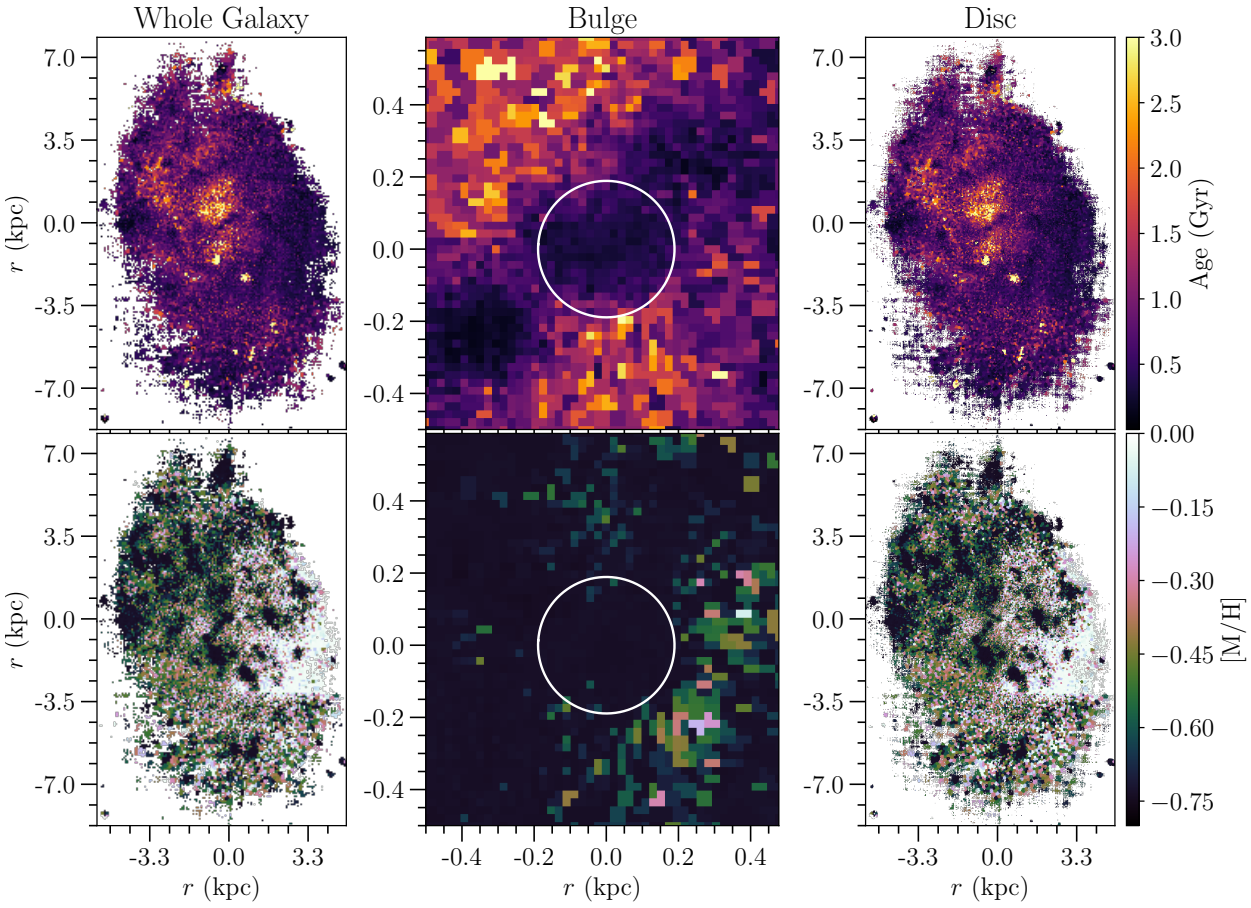

Figure 4: Stellar population maps of NGC1087, plotting the age of the stars (up) and metallicity (down) of each voxel of the different datacubes. From left to right: the whole galaxy, bulge and disc. In order to indicate where the bulge is located at the centre map, we are drawing an ellipse with r_e, $(b/a)_{\rm bulge}$, and $PA_{\rm bulge}$ (see Table 1).

weighted) in each morphological component (in this particular galaxy it is only a disc). To do this we will take into account their shape, that is, we take into account their b/a and their position angle (see Table 1), so we are comparing the radii in an elliptical reference system. In these plots (see Figure 5) we can observe the predominance of young voxels at all radii, with a slight decrease in age towards the outermost radii (we find the fewer older voxels as we move away from the centre and the two columns reaching even older populations must be the two old regions to the south of the centre). As for the metallicity we do not see any radial trend, because as we have seen its gradient is more north-south than radial (see Figure 4). Furthermore, we see a saturation at the highest and lowest values of metallicity. This is nothing but the limits of the SSP models after applying the regularisation. We cannot have values higher or lower than these, but we are sure that these voxels have very high and very low metallicities, respectively. If we go back to Figure 4, we see that the voxels that saturate at low metallicities are almost all from the bursts and at high metallicities are the metal-rich cone on the centre-west, in the rest of the galaxy we find intermediate metallicities.

Recently, the PHANGS-MUSE survey analysed radial gradients of its sample of galaxies (Pessa et al. [2023]), which include NGC1087. They found a trend in the luminosity-weighted age and metallicity of this galaxy (both increasing towards larger radii), but not in the mass-weighted (they

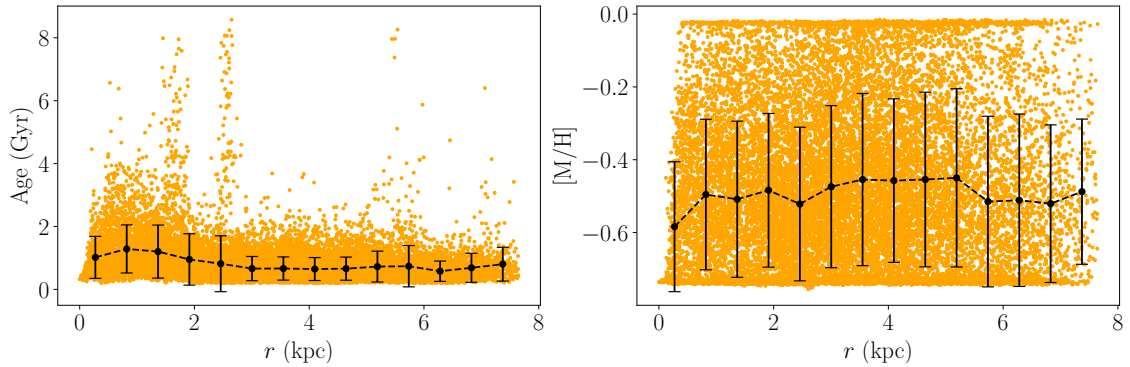

Figure 5: Age (up) and metallicity (down) of each voxel of the disc of NGC1087 (since this galaxy is a pure disc galaxy, the disc is the whole galaxy) at each radius. The radii are defined in an elliptical reference system in the whole galaxy stellar population map (Figure 11), having into account the ellipticity and position angle (see Table 1). The black points are the mean value of the voxels in a given radius range (we divide each plot in 14 regions by radii), and its error is the dispersion of the mean.

also found slightly older populations in the centre, but without a marked trend, like us, but they attribute this to the presence of a bar, and there is no bar in this galaxy as we have checked in the HST images available[5]). They note the special radial behaviour of this galaxy and one other galaxy (NGC1385), which show different trends from the rest (and attribute this to the fact that both are at the low-mass limit of their sample). The values obtained for NGC1087 for age and mass-weighted metallicity in Pessa et al. [2023] are [M/H] $\sim$ -0.4, which is quite consistent with the behaviour observed in the Figure 5, and an age over 3-4 Gyr, which is slightly older than our results.

We are saying that these galaxies are Milky Way-like galaxies, so we can check how much their star formation resembles that of our galaxy. Semenov et al. [2023] suggest that most of the mass in the MW formed more than 10 Gyr ago, so we can see how much mass had formed in our galaxies 10 Gyr ago. Knowing the weight that pPXF gives to each model according to its age and metallicity, we can build the age-metallicity plane (which give us the fraction of stars that formed at each age and metallicity in each voxel, see Appendix A), and integrating in all metallicities, the star formation history (SFH) of each voxel (the number of stars that formed at each age). This SFH can easily be transformed into a cumulative SFH, so that we can see the amount of stellar mass that was created over time until reaching 100% today. With this we can see the fraction of stellar mass that had already formed 10 Gyr ago in each disc with respect to the current one to compare with that assumed for the MW. As NGC1087 is a pure disc galaxy, we perform this analysis for the voxels of the whole galaxy. For our galaxy (see Figure 6) we see that most of the voxels had not formed any of their mass 10 Gyrs ago, and the remaining had only formed less than 20%. It should be noted that the histogram on the right tells us the number of voxels that had formed each mass fraction. This distribution is not representing the total mass distribution of the galaxy, as these voxels have different surface-mass densities and therefore completely different amounts of mass, i.e., the central voxels will have more mass than the outer voxels. It is true that this figure is not a direct comparison with Semenov et al. [2023], but it is also true that, no matter how massive the central voxels are, they almost never reach 20% and never exceed 30% of the current mass, so they

[5] https://hla.stsci.edu/hlaview.html

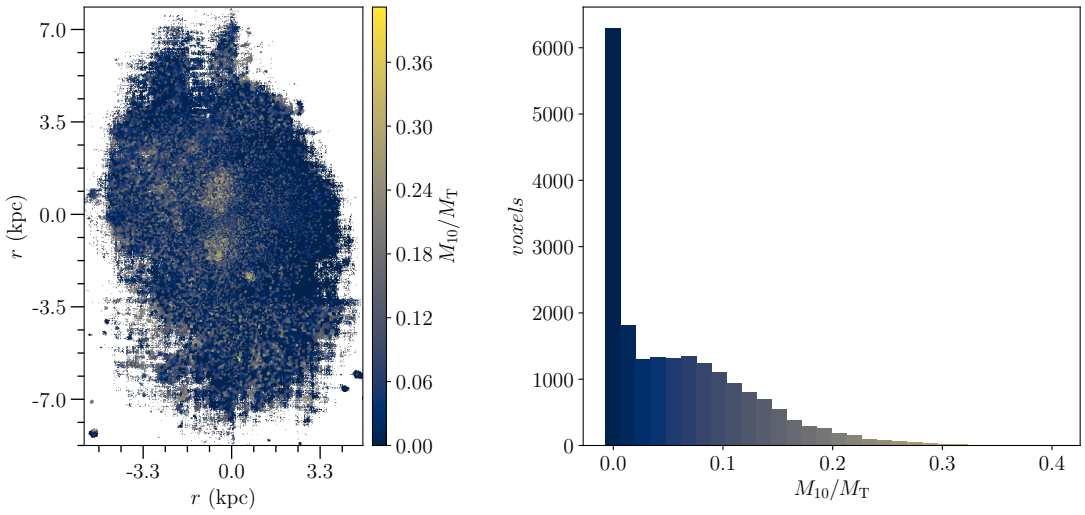

Figure 6: Map with the mass fraction formed in each voxel of the whole galaxy datacube of NGC1087 10 Gyr ago (left) and histogram of the value of this fraction for all voxels (right).

are far from having formed the majority of their mass. Taking this into account, we can say that these results are not compatible from what Semenov et al. [2023] suggests for the Milky Way.

4.3. NGC4598

We now continue with the analysis of NGC4598, which we have fitted using a bulge-bar-disc model in the spectro-photometric decomposition. The fraction of light of each component obtained in the MUSE spectral range are $B/T = 0.168$, $Bar/T = 0.278$ and $D/T = 0.554$, with $B/D = 0.304$. These results seem to indicate that this is not a bulgeless galaxy, but it should be noted that the MUSE FOV does not cover the entire size of the galaxy, so the light coming from the disc will be larger than calculated, and, therefore, the total amount of light will be larger too.

If we observe the results of the spectro-photometric decompositions of each component (see Figure 7) we can see a luminous component in the centre of datacubes for the disc and the bar. This seems like an error in the decompositions, but it can be an unresolved component, like an active galactic nucleus (AGN) or a nuclear stellar cluster (NSC). We can discard an AGN by looking at the central spectrum of the galaxy (see Figure A.2), which has no gas emission lines unlike the spectra of an AGN. Then, it could be a NSC, a dense assemble of stars in the centre of some galaxies. The formation of these components could be due to globular clusters falling into the galaxy centre in galaxies (Neumayer et al. [2020]), which does fit with the lack of gas in Figure A.2. In the datacube of the disc (centre of the Figure 7) we observe another interesting structure, that resembles an x-shaped figure. Erwin and Debattista [2013] suggested by simulations that this kind of structure may be associated with the shape of the isophotes of a boxy peanut. As we have not adjusted these structures in C2D they appear in the datacubes of other components, the boxy-peanut in the disc and the possible NSC in both the disc and the bar.

Now, analysing the mass-weighted stellar populations calculated with pPXF (see Figure 8), we

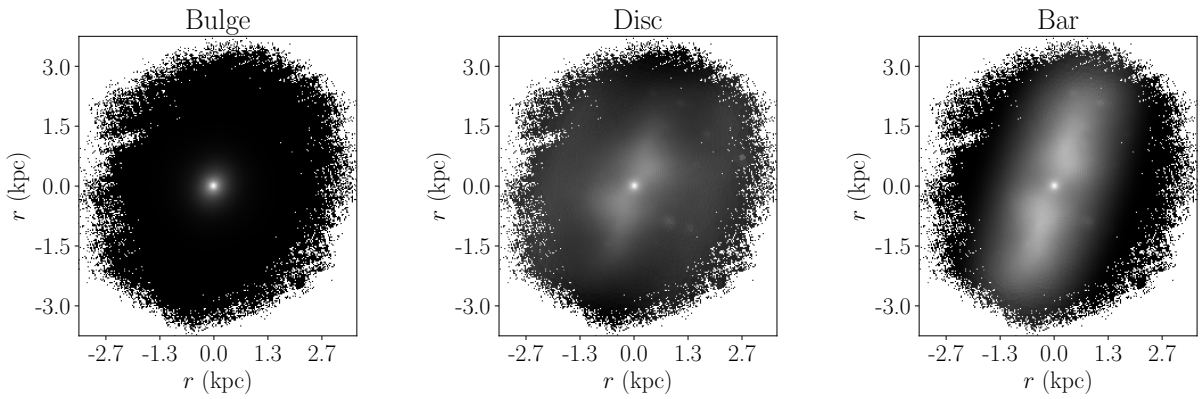

Figure 7: Sum of all the wavelength bins of the datacubes of (from left to right) bulge, disc and bar of NGC4598.

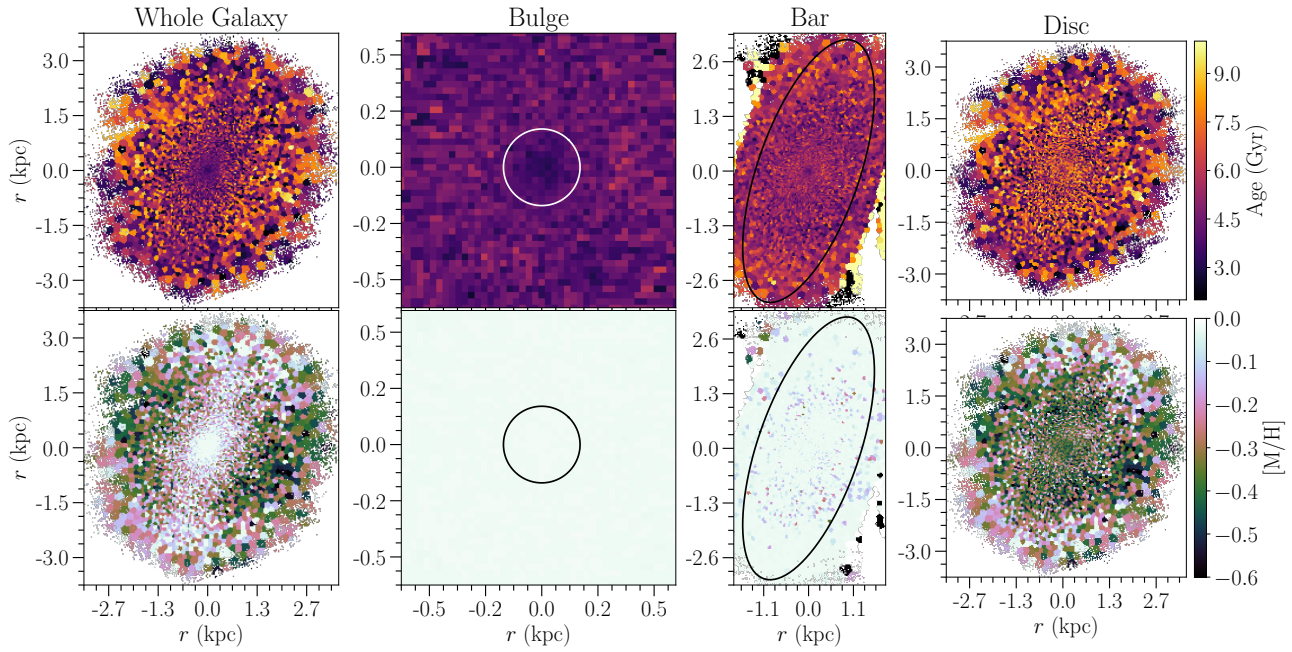

Figure 8: Stellar population maps of NGC4598, plotting the age of the stars (up) and metallicity (down) of each voxel. From left to right: the whole galaxy, bulge, bar and disc. In order to indicate where the bulge and the bar are located at the two centres map, we are plotting ellipses with $r_{\rm e}$, $(b/a)_{\rm bulge}$ and $PA_{\rm bulge}$ for the bulge and $r_{\rm bar}$, $(b/a)_{\rm bar}$ and $PA_{\rm bar}$ for the bar (see Table 1).

observe that NGC4598 has a young bulge, with a young bar too (although with ages somewhat older than the bulge) and a disc with a large dispersion of ages (from young ages like the bulge to much older ages) without any apparent trend. We can see a young small region at the centre of the bar, caused by possible NSC, the bright point in the centre. We don't see it at the disc maybe for the big dispersion of ages. Furthermore, despite observing a boxy structure in the centre of the disc datacube (see Figure 7), we do not see a single age or metallicity structure in the centre of stellar population maps of the disc that would correspond to the boxy-peanut (see Figure 8), whereas we would expect it to have an age similar to that of the bar (as the boxy-peanut is formed from the stars of the bar).

A structure that could also occur in this galaxy is a star formation desert (SFD). This is an area of the disc that fall within the bar radius in which, on some occasions, star formation appears

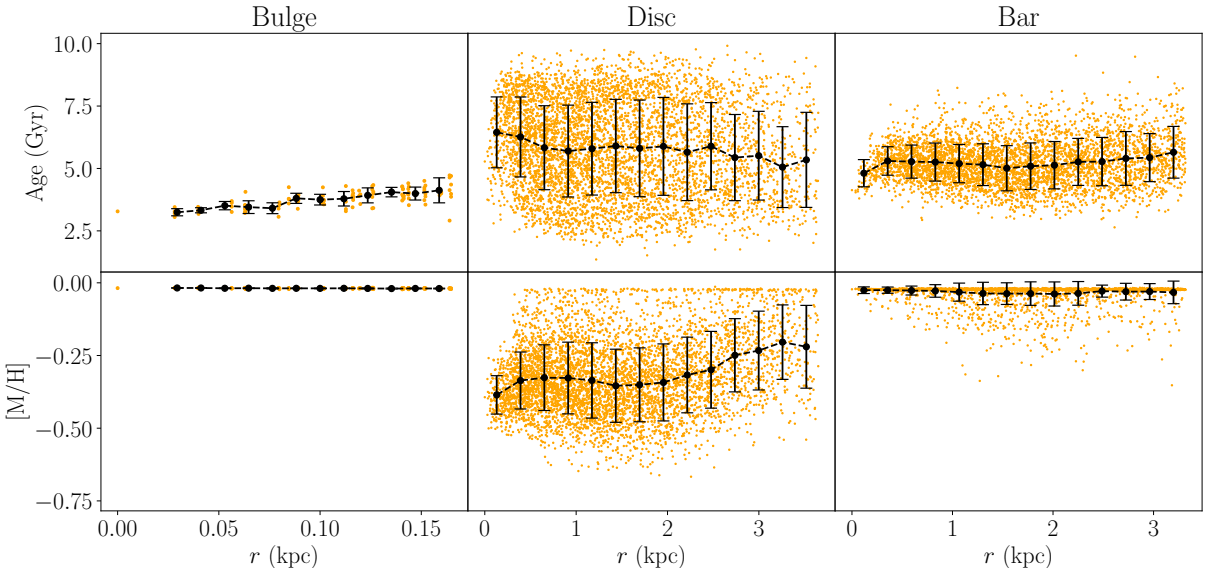

Figure 9: Age (up) and metallicity (down) of each voxel of the (from left to right) bulge, disc and bar of NGC4598 at each radius. The radii are defined in an elliptical reference system in the stellar population maps for each component (Figure 11), having into account the ellipticity and position angle. For the bulge we add voxels up to a radius of r_e and for the bar up to a_{bar} (see Table 1). The black points are the mean value of the voxels in a given radius range (we divide each plot in 14 regions by radii), and its error is the dispersion of the mean.

to stop. This region is supposed to be formed by the dynamics of the bar, and may explain the dispersion of ages in the disc in Figure 8, since the stellar populations of this region are formed by both old stars coming from the bar and young stars that emigrates from the outermost regions of the disc where this star formation has not been detained (Donohoe-Keyes et al. [2019]) The formation of these structures is partially unknown, they form in barred galaxies but not in all of them, and it is not well known what is the factor that delimits when it forms.

Figure 8 shows that the stars in the bar are younger than the older populations in the disc, which does not fit so well with the SFD theory. One possible explanation is that a bar formed in this galaxy when there was still star formation. As stars were forming, their older populations would migrate towards this SFD, leaving a majority of younger, metal-rich populations in the bar, but with somewhat older populations also scattered. Obviously, the younger stars would also migrate to the SFD, but if many more stars formed than there were before, this could explain the predominance of young ages in the bar. In the SFD we do see all ages because the density of stars is much lower and a smaller population of stars can dominate in certain areas.

As we did with NGC1087, now we will observe the radial behaviour of this galaxy in an elliptical reference system (see Figure 9). For the bulge component, we can see a trend towards older ages when moving outwards, while maintaining a high constant metallicity, suggesting star formation from the outside to the inside from the same metal enriched gas. This bulge has young populations (as young as the youngest populations in the disc), so it may have formed from gas that has migrated from the bar or disc towards of the galaxy centre. For the disc we see a large age dispersion, but a slight decrease towards younger ages at larger radii. The gradient may be due to the presence of the boxy-peanut at smaller radii (older age) and the large dispersion across the SFD.

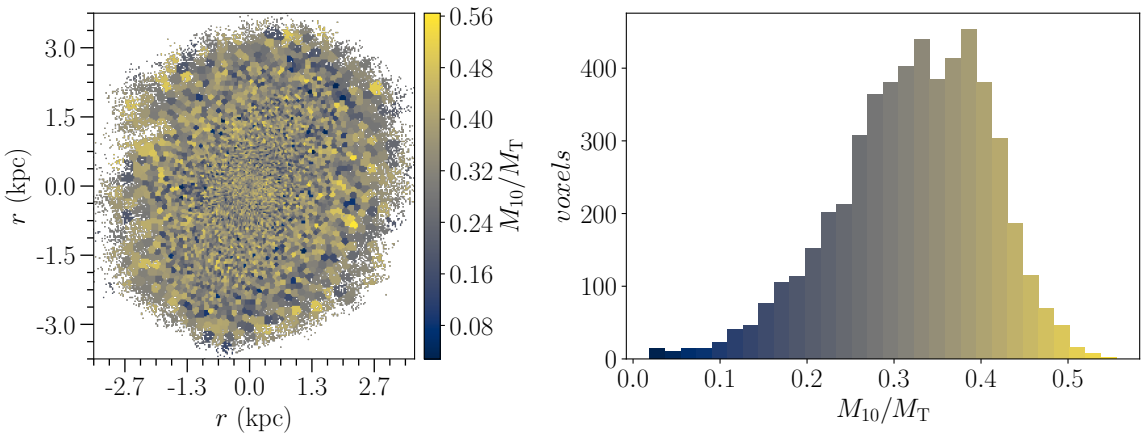

Figure 10: Map with the mass fraction formed in each voxel of the disc datacube of NGC4598 10 Gyr ago (left) and histogram of the value of this fraction for all voxels (right).

In addition, in the metallicity we see an increasing outward gradient, indicating that the younger stars formed from more enriched gas. Finally, in the bar we see a more constant population in age and metallicity (the down in age in the centre is given by the contamination of the young bulge in the spectro-photometric decomposition). It is important to note that the metallicities of the bulge and the bar reach the upper limit, which indicates that this voxels actually have higher metallicities.

If we see the fraction of stellar mass formed 10 Gyr ago in each voxel of the disc (see Figure 10), we see again that almost none of them had formed 50% of its mass at this age. It must be remembered that the distribution of voxels does not have to be related to the distribution of masses (and even more if there is a SFD, having not very dense regions compared to other regions such as the boxy-peanut), so we do not know exactly the total amount of mass that had formed in the disc at that time, but we are sure that it does not reach 50%, so it also does not fulfil what is suggested by Semenov et al. [2023] for the MW.

4.4. NGC5806

The next galaxy to be analysed is NGC5806. As we say in subsection 3.3, despite it present a weak a bar, our FOV is much smaller than the bar radius, so we only fit a bulge-disc galaxy. The fraction of light of each component obtained in the decomposition are $B/T = 0.243$ and $D/T = 0.456$, with $B/D = 0.322$. As before, this values seem a little high with respect to what we expect for a bulgeless Milky Way-like galaxy, but our FOV are not covering all the disc, so the real fraction B/T is smaller. We say in subsection 4.1 that this galaxy has a nuclear disc with a star formation ring. We are not fitting this ring in the spectro-photometric decompositions with C2D, so we see this ring in both datacubes: the disc and the bulge. Not only that, but we can see this ring even in the stellar populations maps (see Figure 11).

Analysing the mass-weighted stellar populations, we see in the Figure 11 that it has an old bulge surrounded by the ring (the star formation ring named before). This ring has some star-forming regions with a lower metallicity than its surroundings, so this galaxy may have had inflows of

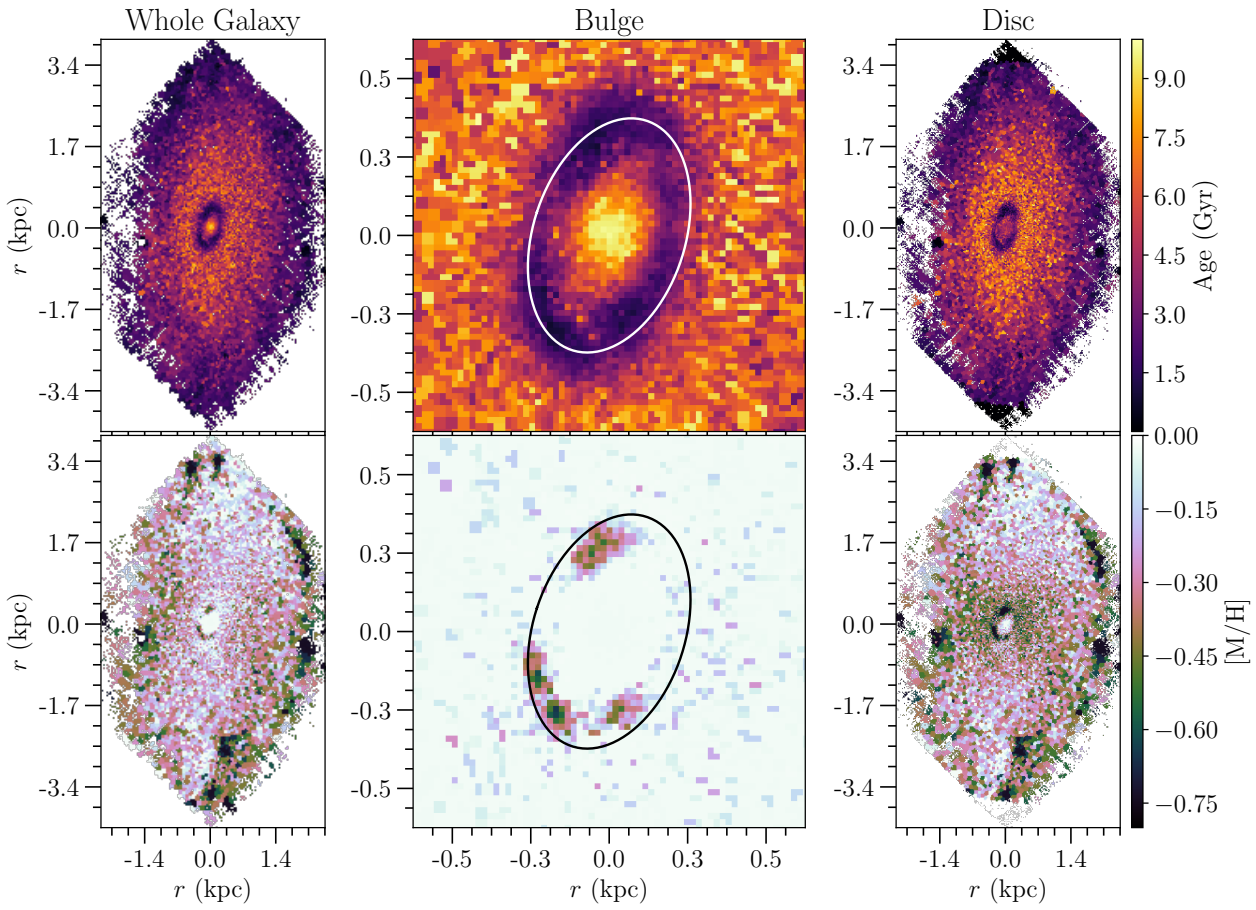

Figure 11: Stellar population maps of NGC5806, plotting the age of the stars (up) and metallicity (down) of each voxel. From left to right: the whole galaxy, bulge and disc. In order to indicate where the bulge is located at the centre map, we are plotting an ellipse with r_e, $(b/a)_{bulge}$ and PA_{bulge} (see Table 1).

low-metallicity gas that settled in parts of this ring. Also, the lower metallicity parts look a little younger than the rest, so it may be that this disc formed first and then (shortly after) this gas arrived. Continuing with the stellar population map of the bulge, we see that the used value of r_e (see Table 1) is right in the middle of the ring. This is possibly a nuclear disc in formation with a star formation ring, the delimitation of whether this ring corresponds to the photometric bulge or not is not so clear, but in the analysis we will continue using this value. Finally, we can see that the disc has slightly higher ages in the centre, which may be due to the fact that, as the bar is not considered in the decomposition, its stars are found together with the disc and these old stars are the stars of the bar.

An interesting thing is that both this galaxy and NGC4598 have a bar, but while in NGC4598 there is evidence of what appears to be a SFD, here we find nothing that makes us indicate this. This is why we said in subsection 4.3 that the formation of a SFD is partially unknown, since even in a sample of only four galaxies and two bars, we found it only in one case. It is true that with this bar we cannot make an analysis as detailed as before to find this possible delimitation of when the SFD is formed and when it is not, but for example, as we said in subsection 3.3, S. Zarattini [in preparation] fitted this galaxy with and without a bar, and found a $b/a = 0.32$ for the bar, while NGC4598 has $b/a = 0.37$ (see Table 1), which makes us indicate that at least in form they are

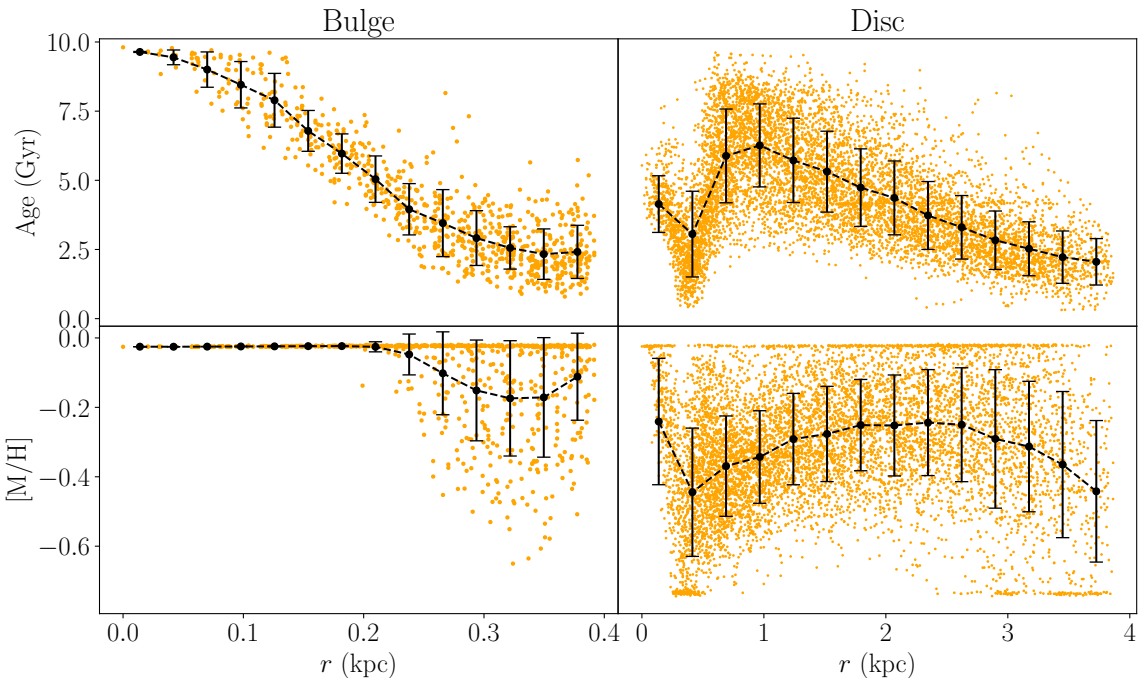

Figure 12: Age (up) and metallicity (down) of each voxel of the bulge (left) and disc (right) of NGC5806 at each radiis. The radii are defined in an elliptical reference system in the stellar population maps for each component (Figure 11), having into account the ellipticity and position angle. For the bulge we add voxels up to a radius of r_e (see Table 1). The black points are the mean value of the voxels in a given radius range (we divide each plot in 14 regions by radii), and its error is the dispersion of the mean.

quite similar, so we cannot give a plausible reason why the SFD is formed.

We will now radially analyse both components (Figure 12). As mentioned before, the star formation ring is present in both components, so we clearly see a drop in age and metallicity. The r_e value of the bulge reaches this ring, so we clearly see a change of populations (with lower age and some lower metallicity) at large bulge radii. Bittner et al. [2020] noted that the nuclear disc have a well-defined radial gradient in ages and metallicities (both decreasing), that is exactly what we see in Figure 12 for the ages. This decreasing ages suggest an inside-out formation from the same gas with the same metallicity, most likely from the star formation ring which is growing and leaving stars inside as part of the nuclear disc. It is true that the metallicities decreases too, but only for the metal-poor populations in the ring. In the inner parts of the bulge the values saturate at maximum metallicity, which means that we do not know exactly the trend in this region. For the disc, once past the ring we see a trend at lower ages as we move away from the centre. In the metallicity we have a high dispersion but seems to be a trend towards higher metallicities but an even larger dispersion at the outskirts of the galaxy. Due to the upper limit of metallicities we don't know if this trend continues. It should again be noted that we have a bar along with the disc, so it is likely that the older populations will belong to the bar.

Let's see now how much mass had been formed in each voxel of the disc 10 Gyr ago. As we see in Figure 13, very little mass in the voxels of the galaxy had formed 10 Gyr ago, with almost no voxels reaching 50%. It is important to re-emphasise that the mass distribution in each voxel is not related to the total mass distribution of the galaxy as they do not have the same surface-mass

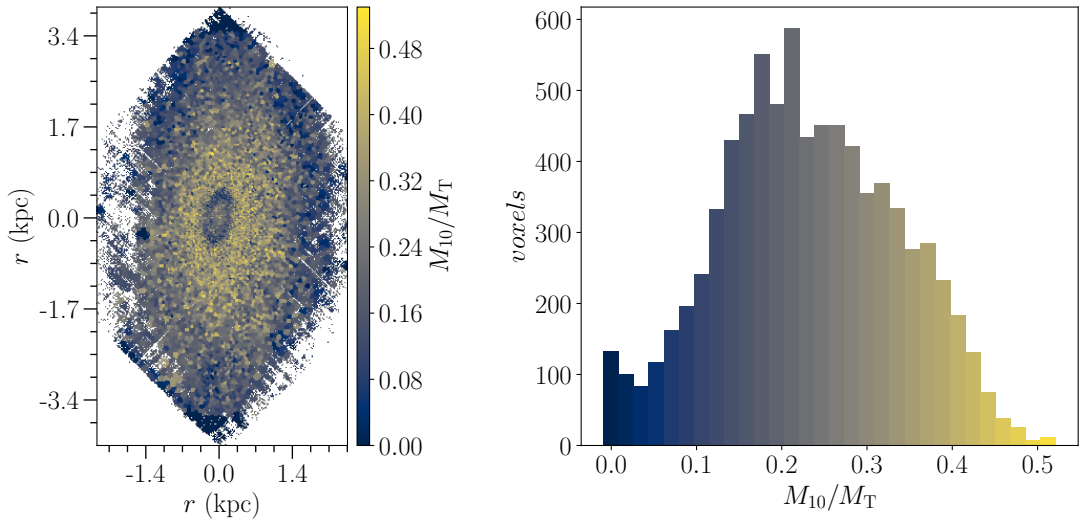

Figure 13: Map with the mass fraction formed in each voxel of the disc datacube of NGC5806 10 Gyr ago (left) and histogram of the value of this fraction for all voxels (right).

densities. In the case of this particular galaxy, the voxels where the most mass formed are in the centre (maybe in the bar), and these voxels have a higher density than the outer ones, so these will weight more in the mass distribution. However, it is also true that as much weight they have on the mass of the galaxy, they had not formed almost 50% of their mass 10 Gyrs ago, so whether they are in the bar or the disc, they are nowhere near having formed the majority of their mass, so the disc of this galaxy is far from what is suggested by Semenov et al. [2023] for the MW, that most of the disc's mass formed 10 Gyrs ago.

4.5. NGC7448

Finally, we will analyse the results of NGC7448. In the decomposition of this galaxy we fit a bulge-disc galaxy, obtaining a fraction of light $B/T = 0.054$ and $D/T = 0.946$, with $B/D = 0.057$, values consistent with a bulgeless galaxy. In the mass-weighted stellar populations of this galaxy (see Figure 14) we see a very young disc with a lot of dispersion of low metallicities together with an older bulge. At the disc we see that the regions of lower metallicity appear to follow a spiral shape, and may be part of the spiral arms. The spectro-photometric decomposition gives us an older bulge than what we seem to see in that region in the whole galaxy. This bulge is undoubtedly the oldest and most metal-rich region in the whole galaxy.

Regarding the analysis of the radial components (see Figure 15), we show that the bulge has old and metal-rich voxels, more than the disc (perhaps some voxels in the central area of the disc are similar in age and metallicity, but they are few). Although we have few voxels, we see a dispersion in ages and metallicities of the bulge without following any trend, indicating that this bulge did not form at once from gas, but may have assembled with existing nearby stars. Regarding the disc, young voxels dominate at all radii, although at smaller radii we see some older population, there are many more young stars. We do not see a clear gradient in age (perhaps a small rise at the beginning for these populations and a drop to a young quasi-continuum), and in metallicities we

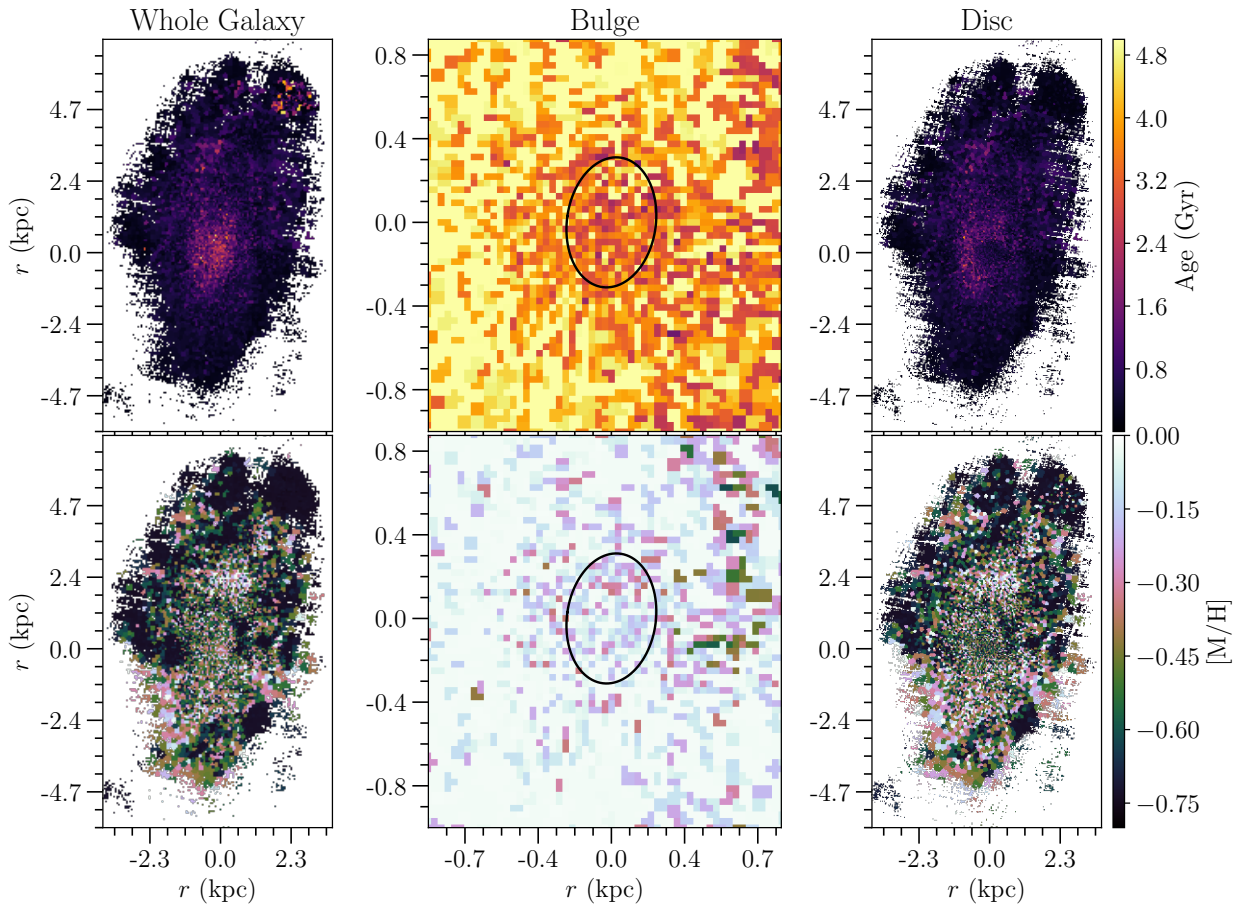

Figure 14: Stellar population maps of NGC7448 obtained with pPXF, plotting the age of the stars (up) and metallicity (down) of each voxel. From left to right: the whole galaxy, bulge and disc. In order to indicate where the bulge is located at the centre map, we are plotting an ellipse with r_e, $(b/a)_{\text{bulge}}$ and PA_{bulge} (see Table 1).

see a rise followed by a drop at mid-radius, but with a high dispersion.

The formation of this galaxy seems uncertain with the data we have. What we know is that it is mostly a very young disc (with a very small bulge), but with some slightly older stars scattered around, without forming a specific region, and mostly with low metallicity stars. It is possible that this galaxy is still forming morphological structures and its bulge is not yet fully defined, since we found some gas (see Figure A.4) that indicates existing star formation in the bulge. Let's also remember that the datacubes of this galaxy have had to be readjusted, removing its gas component due to the strong emission lines in the disc that made the bulge disappear at H_β, so it has a lot of star formation. We can affirm that it is a very young galaxy with a lot of current stellar formation.

Finally, we can see in Figure 16 that, like in NGC1087, almost none of the voxels of the galaxy had formed any of its mass 10 Gyr ago, making it impossible to compare with the MW as indicated by Semenov et al. [2023] (that the most of the mass of the MW disc was formed 10 Gyr ago). This fits with what was explained before, that it is a really young galaxy with a lot of current star formation. It is true that there were already some stars that are now part of the galaxy formed 10 Gyr ago, but the voxels that contain these stars are very few and do not even reach 20% of the mass formed 10 Gyr ago. Furthermore, these voxels do not seem to occupy a special region in the galaxy,

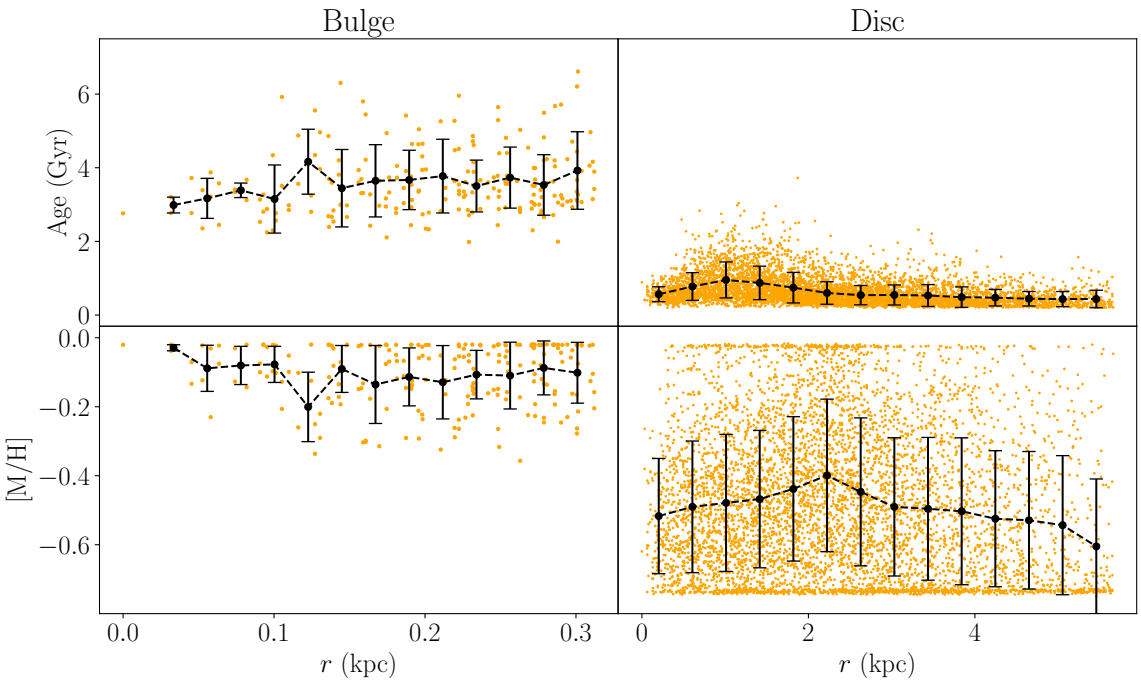

Figure 15: Age (up) and metallicity (down) of each voxel of the bulge (left) and disc (right) of NGC5806 at each radius. The radii are defined in an elliptical reference system in the stellar population maps for each component (Figure 11), having into account the ellipticity and position angle. For the bulge we add voxels up to a radius of r_e (see Table 1). The black points are the mean value of the voxels in a given radius range (we divide each plot in 14 regions by radii), and its error is the dispersion of the mean.

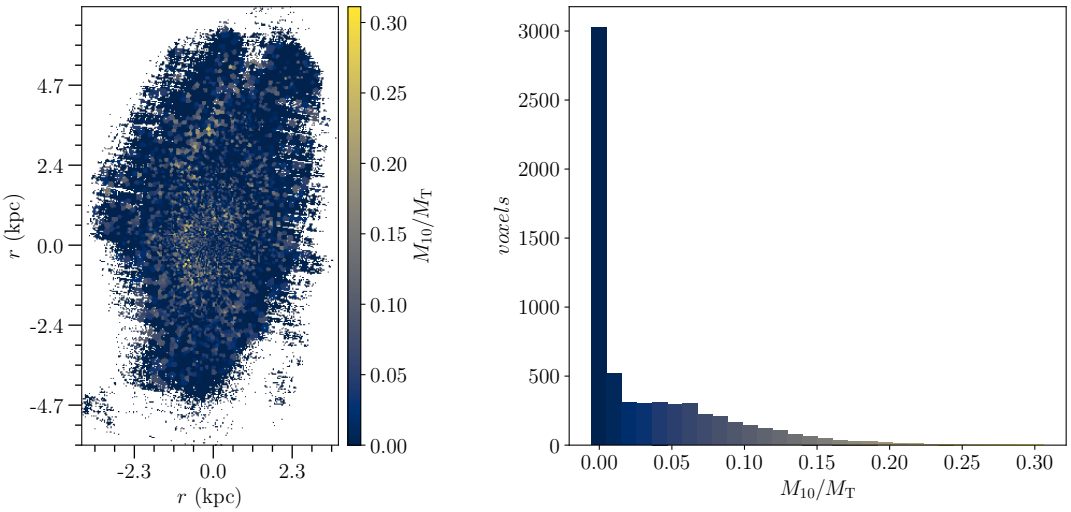

Figure 16: Map with the mass fraction formed in each voxel of the disc datacube of NGC57448 10 Gyr ago (left) and histogram of the value of this fraction for all voxels (right).

we found some in the centre and perhaps a few others forming a spiral, but very interspersed with voxels that had no mass yet 10 Gyr ago.

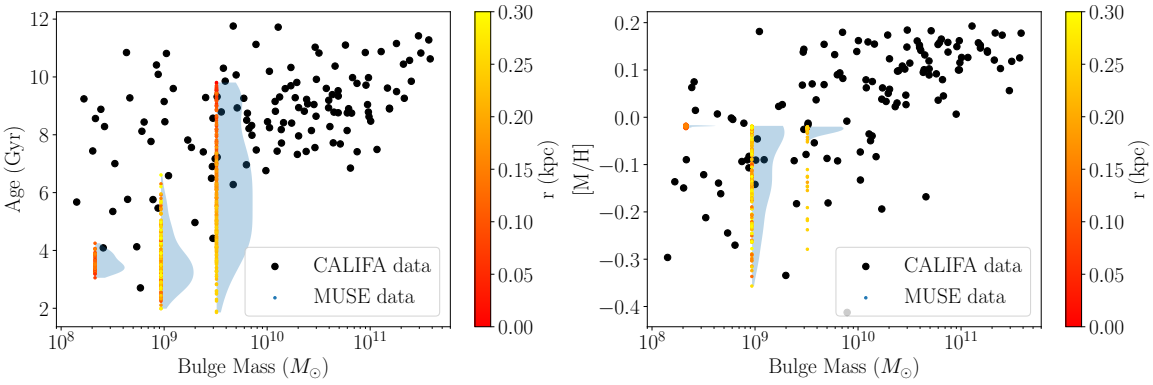

Figure 17: Comparison of the age (left) and metallicities (right) of our bulges and the CALIFA bulges (A. de Lorenzo-Caceres et al. [in preparation]) depending on their masses obtained by S. Zarattini et al. [in preparation]. Our galaxies are, from less to more massive, NGC4598, NGC7448 and NGC5806. For our galaxies we plot all the voxels of our bulge maps (smaller than r_e, see Table 1) and use a range of colours depending on the distance of each voxel from the centre (in kpc), in order to compare the properties at different radii. The blue area to the right of the data for our bulges indicates the number of voxels for each value of each property.

4.6. Comparision with CALIFA data

Finally, we can compare our results with the spectro-photometric decompositions of the CALIFA sample (Méndez-Abreu et al. [2021]), to look for differences between the bulges in a "bulgeless" galaxy and in a "normal" galaxy, as well as to better understand the formation of the bulgeless galaxies. For this, we compare the age and metallicity of the bulges depending on their masses. We will use the masses of our bulges which were derived by S. Zarattini et al. [in preparation]. They perform the photometric decompositions with GASP2D for the SDSS images of BEARD galaxies and derive the masses of their bulges using the total bulge luminosities and their colours. The masses obtained are:

- NGC1087: 1.81×10^8 $M_\odot$.
- NGC4598: 2.13×10^8 $M_\odot$.
- NGC5806: 3.22×10^9 $M_\odot$.
- NGC7448: 9.13×10^8 $M_\odot$.

They also performed a disc-bulge analysis of NGC1087, but we have determined that this central component is not a bulge, so we will not include it in the comparison with CALIFA. The masses and properties of the bulges in the CALIFA sample were obtained by A. de Lorenzo-Caceres et al. [in preparation], where they analyse a sample of 129 galaxies. In these galaxies, they carried out a study of populations using the PIPE3D pipeline (Sánchez et al. [2015]) in their different morphological components. They have also studied the discs of these galaxies, but we cannot compare them with ours because we do not have the masses of our discs (those of the bulges we only have from previous work carried out within the BEARD team), so we will focus only on in the comparison of the bulges.

In the data of the CALIFA bulges (see Figure 17) we see that the most massive bulges tend to be older and more metal-rich, converging more and more as the mass increases, while we find

a greater dispersion of age and metallicity values for young bulges. Our bulges, as expected, are low-massive bulges (being a sample of bulgeless galaxies, we hope that if we find one, it will be low-massive), but the data on the different properties fall within the dispersion of the data of CALIFA. For NGC7448 and NGC4598, the less massive ones, we found that these bulges are young and metal-rich (In NGC7448 we found greater dispersion in the values of the voxels, but most of them are found in similar values to NGC4598). On the other hand, in NGC5806 we have a much greater dispersion of ages due to the presence of the star formation ring around the older nuclear disc. Despite this dispersion, all the values (especially the most central ones, not so much the ring) fall within the dispersion of the age values of the CALIFA bulges. We must emphasize that it is possible that our bulges have a higher metallicity, because the values of the three were close to the limit of the models with which we compared them.

5. Conclusions and future work

In this work we have study the paths of formation of massive bulgeless galaxies from the BEARD sample. The existence of these galaxies and the large number in the nearby universe pose a problem for the ΛCDM model. In addition, recent studies indicate that the Milky Way is one of these bulgeless galaxies (Shen et al. [2010]), so understanding the formation and existence of these galaxies could help us understand the formation of our own galaxy. With this purpose we study four galaxies within the BEARD sample, performing a spectro-photometric analysis with C2D (Méndez-Abreu et al. [2019]) and analysing their mass-weighted populations with pPXF Cappellari and Emsellem [2004]). In this study we found different stellar populations and structures en each galaxy:

- NGC1087: We perform the spectro-photometric decomposition using a bulge-disc model, but we found that is a pure disc galaxy. This galaxy is composed by a very young disc which has many bursts of star formation, as well as a north-south metallicity gradient, possibly because it is undergoing a merger in its southern zone (which has been found by another study within the project BEARD). Regarding the radial trend of age and metallicity, we found some slightly older populations in the centre but no remarkable trend in either age or metallicity (because the trend of metallicity is north-south, not radial). In a PHANGS-MUSE study (Pessa et al. [2023]) they also analysed this galaxy and found no trend in these mass-weighted parameters. They attributed the presence of older populations near to the centre to the presence of a bar, but we did not find any evidence that it could exist.

- NGC4598: We perform the spectro-photometric decomposition using a bulge-bar-disc model. We found a non-resolved component in the centre of each component, that may be a NSC. In the disc we found another structure that seems like a boxy-peanut. Regarding the stellar populations, we find that this galaxy has a very young and metal-rich bulge (with a formation from the outside in), a bar that is also metal-rich and young (but older than the bulge), and a disc with a great dispersion of ages and metallicities, reaching populations much older than those of the bar and bulge. This observed dispersion can be attributed to an SFD (Donohoe-Keyes et al. [2019]) caused by the dynamics of the bar.

- NGC5806: We perform the spectro-photometric decomposition using a bulge-disc model, but we know that this galaxy has a bar much larger than our FOV. This galaxy also have a nuclear disc with a star formation ring surrounding (which is seen in the results of the decomposition of both the bulge and the disc), and we can affirm that due to the fact that the kinematics and the stellar populations match with those expected from this structure (Bittner et al. [2020]). In the stellar populations we found an older bulge with a smooth decreasing trend towards the ring of star formation with a high metallicity. On the disc we also find a decreasing trend in ages and increasing in metallicities once we pass the ring. In addition, we found an older population in the central zone of the disc, which must be part of the unfitted bar.

- NGC7448: This galaxy has a lot of star formation because of the large amount of emission all over the disc. This has even been a problem with the spectro-photometric decomposition, as in some lines like H_β the bulge seemed to disappear, so we had to adjust the gas with pPXF and remove it from the datacube. After this treatment, we perform the spectro-photometric decomposition using a bulge-disc model. This galaxy has a very young and metal-poor disc, with a somewhat older bulge. This bulge, unlike the rest, presents a radial dispersion in ages and metallicities, without following any trend, possibly due to the fact that, being so young, its populations may not have settled yet.

It is important to note that our metallicities have an upper and lower limit due to the regularization applied in the pPXF modelling. A future advance for this work to improve the results of the stellar populations would be to perform simulations to understand better the effect of regularization in order to carry out a better analysis of the metallicities.

In a comparison with the data of the sample bulges from CALIFA (A. de Lorenzo-Cáceres et al. [in preparation]), we see that our bulges, as we expected, are not very massive. The CALIFA bulges analysed by this study show a dispersion of age and metallicity values for low-mass bulges, and the values of our bulges are within this dispersion, they do not present any special behaviour. A good future advance for this work would be to derivate the masses of the discs to also be able to compare with what was obtained in the CALIFA survey and be able to check possible special characteristics of these discs.

Finally, in order to compare the history of these galaxies with that of the MW, Semenov et al. [2023] suggest that most of the stellar mass of the MW formed 10 Gyr ago. In our galaxies, almost no voxel had reached 50% of its mass 10 Gyr ago. In some cases, such as NGC1087 and NGC7448, almost none of the voxels had not formed any of the mass 10 Gyr ago. Therefore, we can affirm that the stellar mass of our galaxies did not form in the same way as this study suggests for the MW.

Our 4 galaxies present, for the most part, very young discs. Perhaps NGC4598 is an exception, but if there is a SFD we would not be seeing the rest of the disc and we cannot confirm it. Furthermore, as we see in Figure 10, almost no voxel of the disc had formed 50% of its mass 10 Gyr ago, so it can also be considered young. But apart from these young discs, they have nothing in common as far as structure is concerned. One presents a bar with SFD, another presents a nuclear disc with a ring of star formation (with a bar too, but without SFD) and another is a pure disc. We have different morphologies with different histories, but they are all bulgeless galaxies, so one thing we can say: there is no single path for the formation of these bulgeless galaxies.

References

Vladimir Avila-Reese, Jesú s Zavala, and Ivan Lacerna. The growth of galactic bulges through mergers in $\{Lambda$ cold dark matter haloes revisited – II. morphological mix evolution. *Monthly Notices of the Royal Astronomical Society*, 441(1):417–430, apr 2014. doi: 10.1093/mnras/stu382. URL https://doi.org/10.1093%2Fmnras%2Fstu382.

Fabio D. Barazza, Shardha Jogee, and Irina Marinova. Bars in disk-dominated and bulge-dominated galaxies atiz/i∼ 0: New insights from ∼3600 SDSS galaxies. *The Astrophysical Journal*, 675 (2):1194–1212, mar 2008. doi: 10.1086/526510. URL https://doi.org/10.1086%2F526510.

Adrian Bittner, Patricia Sánchez-Blázquez, Dimitri A. Gadotti, Justus Neumann, Francesca Fragkoudi, Paula Coelho, Adriana de Lorenzo-Cáceres, Jesús Falcón-Barroso, Taehyun Kim, Ryan Leaman, Ignacio Martín-Navarro, Jairo Méndez-Abreu, Isabel Pérez, Miguel Querejeta, Marja K. Seidel, and Glenn van de Ven. Inside-out formation of nuclear discs and the absence of old central spheroids in barred galaxies of the TIMER survey. , 643:A65, November 2020. doi: 10.1051/0004-6361/202038450.

Massimo Capaccioli. Photometry of early-type galaxies and the r1/4 law. In Harold G. Corwin and Lucette Bottinelli, editors, *The World of Galaxies*, pages 208–228, New York, NY, 1989. Springer US. ISBN 978-1-4613-9356-6.

Michele Cappellari. Full spectrum fitting with photometry in ppxf: non-parametric star formation history, metallicity and the quenching boundary from 3200 LEGA-C galaxies at redshift z∽0.8. *arXiv e-prints*, art. arXiv:2208.14974, August 2022. doi: 10.48550/arXiv.2208.14974.

Michele Cappellari and Yannick Copin. Adaptive spatial binning of integral-field spectroscopic data using Voronoi tessellations. , 342(2):345–354, June 2003. doi: 10.1046/j.1365-8711.2003.06541.x.

Michele Cappellari and Eric Emsellem. Parametric Recovery of Line-of-Sight Velocity Distributions from Absorption-Line Spectra of Galaxies via Penalized Likelihood. , 116(816):138–147, February 2004. doi: 10.1086/381875.

Andrea Cimatti, Filippo Fraternali, and Carlo Nipoti. *Introduction to Galaxy Formation and Evolution*. Cambridge University Press, Cambridge, UK, 2019. ISBN 978-1107056070.

R. E. de Souza, D. A. Gadotti, and S. dos Anjos. BUDDA: A New Two-dimensional Bulge/Disk Decomposition Code for Detailed Structural Analysis of Galaxies. , 153(2):411–427, August 2004. doi: 10.1086/421554.

Gérard de Vaucouleurs. *Classification and Morphology of External Galaxies*. Springer, Berlin, 1959.

C E Donohoe-Keyes, M Martig, P A James, and K Kraljic. Redistribution of stars and gas in the star formation deserts of barred galaxies. *Monthly Notices of the Royal Astronomical Society*,

489(4):4992–5003, sep 2019. doi: 10.1093/mnras/stz2474. URL https://doi.org/10.1093%2Fmnras%2Fstz2474.

Emsellem, Eric, Schinnerer, Eva, Santoro, Francesco, Belfiore, Francesco, Pessa, Ismael, McElroy, Rebecca, Blanc, Guillermo A., Congiu, Enrico, Groves, Brent, Ho, I-Ting, Kreckel, Kathryn, Razza, Alessandro, Sanchez-Blazquez, Patricia, Egorov, Oleg, Faesi, Chris, Klessen, Ralf S., Leroy, Adam K., Meidt, Sharon, Querejeta, Miguel, Rosolowsky, Erik, Scheuermann, Fabian, Anand, Gagandeep S., Barnes, Ashley T., Besli´c, Ivana, Bigiel, Frank, Boquien, Médéric, Cao, Yixian, Chevance, Mélanie, Dale, Daniel A., Eibensteiner, Cosima, Glover, Simon C. O., Grasha, Kathryn, Henshaw, Jonathan D., Hughes, Annie, Koch, Eric W., Kruijssen, J. M. Diederik, Lee, Janice, Liu, Daizhong, Pan, Hsi-An, Pety, Jérôme, Saito, Toshiki, Sandstrom, Karin M., Schruba, Andreas, Sun, Jiayi, Thilker, David A., Usero, Antonio, Watkins, Elizabeth J., and Williams, Thomas G. The phangs-muse survey - probing the chemo-dynamical evolution of disc galaxies. *A&A*, 659:A191, 2022. doi: 10.1051/0004-6361/202141727. URL https://doi.org/10.1051/0004-6361/202141727.

Peter Erwin. IMFIT: A Fast, Flexible New Program for Astronomical Image Fitting. , 799(2):226, February 2015. doi: 10.1088/0004-637X/799/2/226.

Peter Erwin and Victor P. Debattista. Peanuts at an angle: detecting and measuring the three-dimensional structure of bars in moderately inclined galaxies. , 431(4):3060–3086, June 2013. doi: 10.1093/mnras/stt385.

Norman Macleod Ferrers. *An Elementary Treatise on Spherical Harmonics and Subjects Connected with Them*. Macmillan and Co., 1877.

K. C. Freeman. On the Disks of Spiral and S0 Galaxies. , 160:811, June 1970. doi: 10.1086/150474.

Alister W. Graham and Simon P. Driver. A concise reference to (projected) sérsic ir/isup1/in/i/sup quantities, including concentration, profile slopes, petrosian indices, and kron magnitudes. *Publications of the Astronomical Society of Australia*, 22(2):118–127, 2005. doi: 10.1071/as05001. URL https://doi.org/10.1071%2Fas05001.

Edwin Hubble. *The Realm of Nebulae*. Yale University Press, New Haven, 1936.

Evelyn J. Johnston, Boris Häußler, Alfonso Aragón-Salamanca, Michael R. Merrifield, Steven Bamford, Matthew A. Bershady, Kevin Bundy, Niv Drory, Hai Fu, David Law, Christian Nitschelm, Daniel Thomas, Alexandre Roman Lopes, David Wake, and Renbin Yan. SDSS-IV MaNGA: bulge-disc decomposition of IFU data cubes (BUDDI). , 465(2):2317–2341, February 2017. doi: 10.1093/mnras/stw2823.

John Kormendy, Niv Drory, Ralf Bender, and Mark E. Cornell. BULGELESS GIANT GALAXIES CHALLENGE OUR PICTURE OF GALAXY FORMATION BY HIERARCHICAL CLUSTERING,. *The Astrophysical Journal*, 723(1):54–80, oct 2010. doi: 10.1088/0004-637x/723/1/54. URL https://doi.org/10.1088%2F0004-637x%2F723%2F1%2F54.

P. Kroupa. On the variation of the initial mass function. *Monthly Notices of the Royal Astronomical Society*, 322(2):231–246, apr 2001. doi: 10.1046/j.1365-8711.2001.04022.x. URL https://doi.org/10.1046%2Fj.1365-8711.2001.04022.x.

Eija Laurikainen, Heikki Salo, and Ronald Buta. Multicomponent decompositions for a sample of S0 galaxies. , 362(4):1319–1347, October 2005. doi: 10.1111/j.1365-2966.2005.09404.x.

J. Méndez-Abreu, J. A. L. Aguerri, E. M. Corsini, and E. Simonneau. Structural properties of disk galaxies. I. The intrinsic equatorial ellipticity of bulges. , 478(2):353–369, February 2008. doi: 10.1051/0004-6361:20078089.

J. Méndez-Abreu, T. Ruiz-Lara, L. Sánchez-Menguiano, A. de Lorenzo-Cáceres, L. Costantin, C. Catalán-Torrecilla, E. Florido, J. A. L. Aguerri, J. Bland-Hawthorn, E. M. Corsini, R. J. Dettmar, L. Galbany, R. García-Benito, R. A. Marino, I. Márquez, R. A. Ortega-Minakata, P. Papaderos, S. F. Sánchez, P. Sánchez-Blazquez, K. Spekkens, G. van de Ven, V. Wild, and B. Ziegler. Two-dimensional multi-component photometric decomposition of CALIFA galaxies. , 598:A32, February 2017. doi: 10.1051/0004-6361/201629525.

J. Méndez-Abreu, S. F. Sánchez, and A. de Lorenzo-Cáceres. Spectro-photometric decomposition of galaxy structural components. *Monthly Notices of the Royal Astronomical Society*, 484(3): 4298–4314, jan 2019. doi: 10.1093/mnras/stz276. URL https://doi.org/10.1093%2Fmnras%2Fstz276.

J. Méndez-Abreu, A. de Lorenzo-Cáceres, and S. F. Sánchez. The origin of bulges and discs in the CALIFA survey - I. Morphological evolution. , 504(2):3058–3073, June 2021. doi: 10.1093/mnras/stab1064.

Julio F. Navarro, Carlos S. Frenk, and Simon D. M. White. The Structure of Cold Dark Matter Halos. , 462:563, May 1996. doi: 10.1086/177173.

Nadine Neumayer, Anil Seth, and Torsten Böker. Nuclear star clusters. , 28(1):4, July 2020. doi: 10.1007/s00159-020-00125-0.

Chien Y. Peng, Luis C. Ho, Chris D. Impey, and Hans-Walter Rix. Detailed Structural Decomposition of Galaxy Images. , 124(1):266–293, July 2002. doi: 10.1086/340952.

I. Pessa, E. Schinnerer, P. Sanchez-Blazquez, F. Belfiore, B. Groves, E. Emsellem, J. Neumann, A. K. Leroy, F. Bigiel, M. Chevance, D. A. Dale, S. C. O. Glover, K. Grasha, R. S. Klessen, K. Kreckel, J. M. D. Kruijssen, F. Pinna, M. Querejeta, E. Rosolowsky, and T. G. Williams. Resolved stellar population properties of PHANGS-MUSE galaxies. *Astronomy &amp Astrophysics*, 673:A147, may 2023. doi: 10.1051/0004-6361/202245673. URL https://doi.org/10.1051%2F0004-6361%2F202245673.

Adriano Pietrinferni, Santi Cassisi, Maurizio Salaris, and Fiorella Castelli. A large stellar evolution database for population synthesis studies. II. stellar models and isochrones for an -enhanced metal distribution. *The Astrophysical Journal*, 642(2):797–812, may 2006. doi: 10.1086/501344. URL https://doi.org/10.1086%2F501344.

J. Richard, R. Bacon, J. Vernet, D. Wylezalek, E. Valenti, F. Selman, F. Bian, and E. Johnston. *MUSE User Manual*. European Southern Observatory (ESO), 2021. Doc. version 12.2. Doc. number ESO-261650.

Vadim A. Semenov, Charlie Conroy, Vedant Chandra, Lars Hernquist, and Dylan Nelson. Formation of galactic disks i: Why did the milky way's disk form unusually early? 2023.

J. L. Sérsic. Influence of the atmospheric and instrumental dispersion on the brightness distribution in a galaxy. *Boletin de la Asociacion Argentina de Astronomia La Plata Argentina*, 6:41–43, February 1963.

Juntai Shen, R. Michael Rich, John Kormendy, Christian D. Howard, Roberto De Propris, and Andrea Kunder. Our Milky Way as a Pure-disk Galaxy—A Challenge for Galaxy Formation. , 720(1):L72–L76, September 2010. doi: 10.1088/2041-8205/720/1/L72.

Kyle R. Stewart, James S. Bullock, Risa H. Wechsler, and Ariyeh H. Maller. Gas-rich Mergers in LCDM: Disk Survivability and the Baryonic Assembly of Galaxies. , 702(1):307–317, September 2009. doi: 10.1088/0004-637X/702/1/307.

S. F. Sánchez, E. Pérez, P. Sánchez-Blázquez, J. J. González, F. F. Rosales-Ortega, M. Cano-Díaz, C. López-Cobá, R. A. Marino, A. Gil de Paz, M. Mollá, A. R. López-Sánchez, Y. Ascasibar, and J. Barrera-Ballesteros. Pipe3d, a pipeline to analyze integral field spectroscopy data: I. new fitting phylosophy of fit3d, 2015.

A. Vazdekis, M. Koleva, E. Ricciardelli, B. Röck, and J. Falcón-Barroso. UV-extended E-MILES stellar population models: young components in massive early-type galaxies. , 463(4):3409–3436, December 2016. doi: 10.1093/mnras/stw2231.

A. pPXF adjustments in central voxels

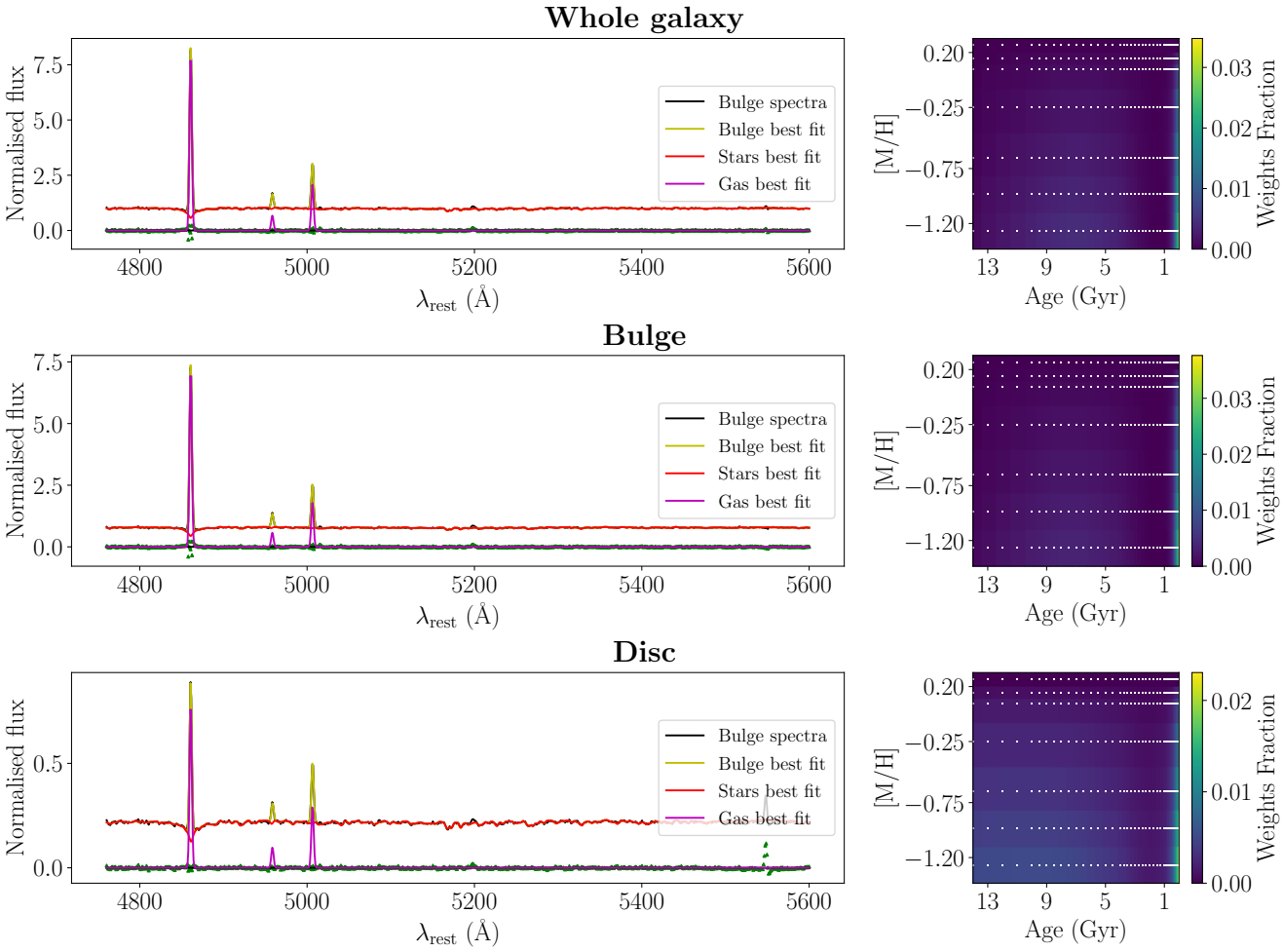

Figure A.1: Fit obtained with pPXF of the spectra (left) and age-metallicity plane (right) of central voxel of (from up tu down) the whole galaxy, the bulge and the disc of NGC1087. In the spectrum adjustment (left) we plot: the spectra of those central voxels of each datacubes (black), the best fit of pPXF with the different models for the stars (red) and for the gas (purple), the sum of both (yellow) and the residual of the fits with the spectrum (green scatter). The flux has been normalised to the value of the spectrum continuum of the whole galaxy (top). In the age-metallicity plane (left) we plot the weights of each model to fit the ages and metallicities of the stars (red spectrum). Each white point in this plot is a model with a different age and metallicity. Despite the fact that we have concluded that this galaxy has no bulge and the whole galaxy would already correspond to the disc, we put the fittings made for all datacubes to show why we have concluded that.

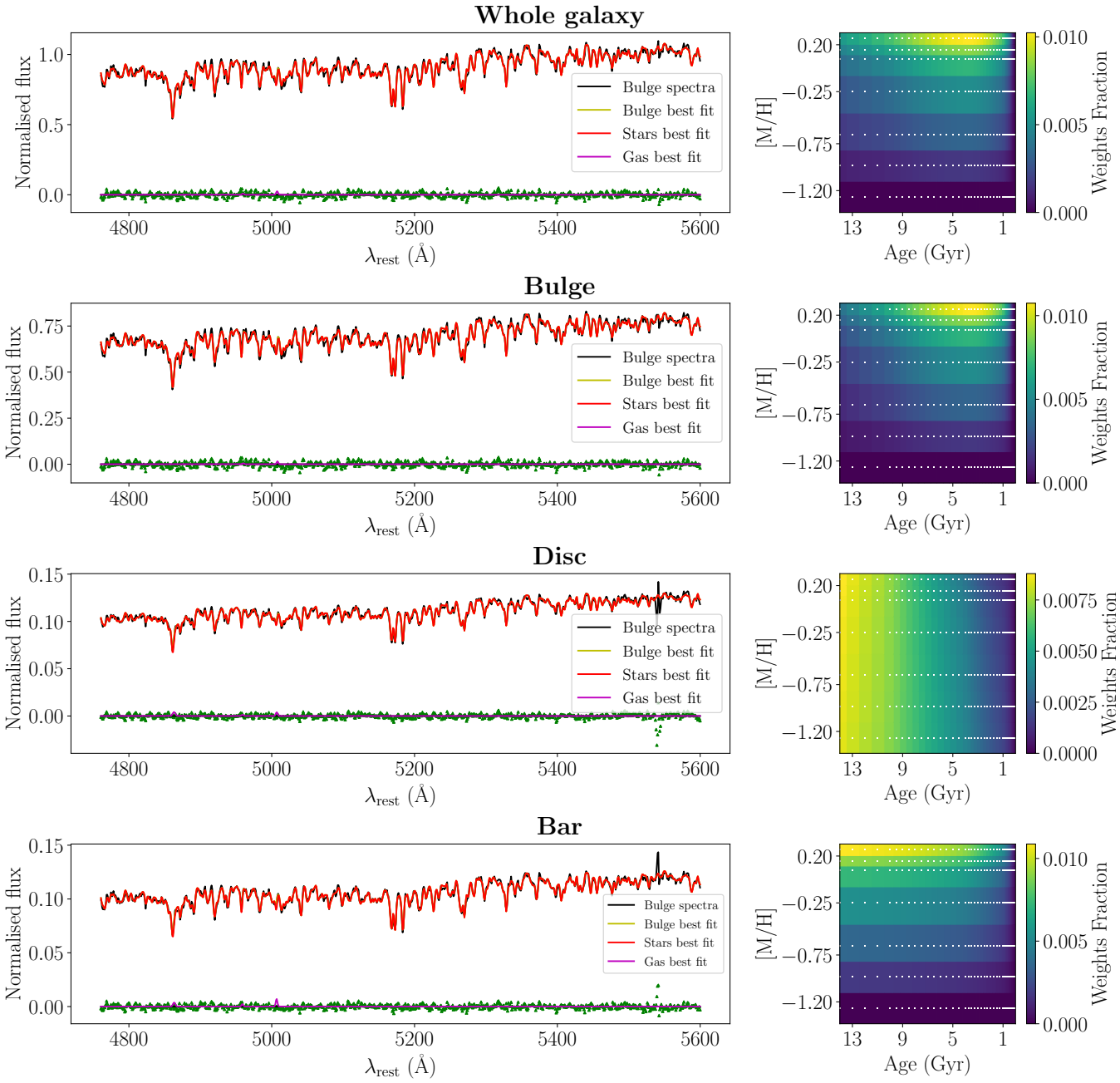

Figure A.2: Fit obtained with pPXF of the spectra (left) and age-metallicity plane (right) of central voxel of (from up tu down) the whole galaxy, the bulge, the disc and the bar of NGC4598. In the spectrum adjustment (left) we plot: the spectra of those central voxels of each datacubes (black), the best fit of pPXF with the different models for the stars (red) and for the gas (purple), the sum of both (yellow) and the residual of the fits with the spectrum (green scatter). The flux has been normalised to the value of the spectrum continuum of the whole galaxy (top). In the age-metallicity plane (left) we plot the weights of each model to fit the ages and metallicities of the stars (red spectrum). Each white point in this plot is a model with a different age and metallicity.

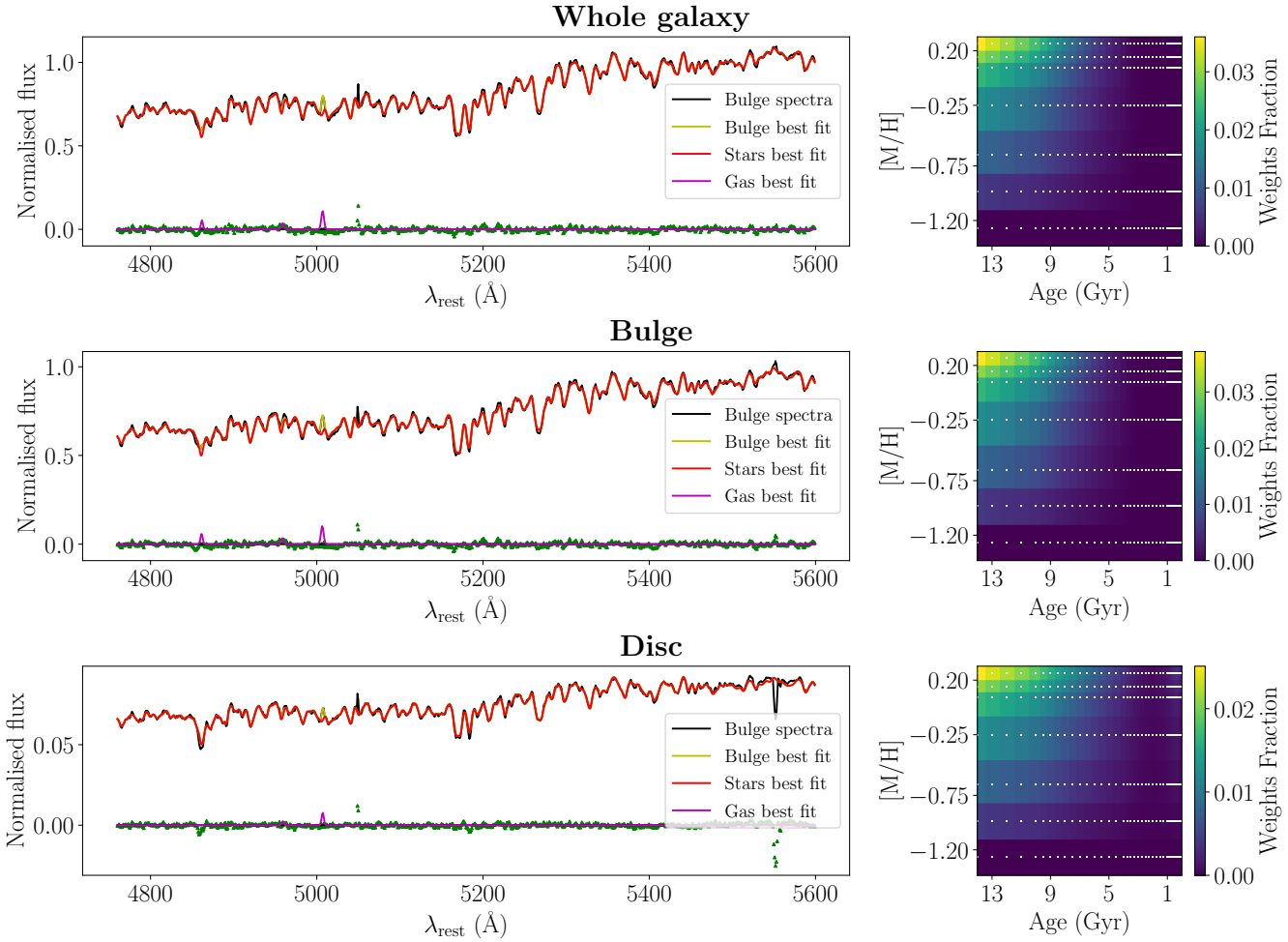

Figure A.3: Fit obtained with pPXF of the spectra (left) and age-metallicity plane (right) of central voxel of (from up tu down) the whole galaxy, the bulge and the disc of NGC5806. In the spectrum adjustment (left) we plot: the spectra of those central voxels of each datacubes (black), the best fit of pPXF with the different models for the stars (red) and for the gas (purple), the sum of both (yellow) and the residual of the fits with the spectrum (green scatter). The flux has been normalised to the value of the spectrum continuum of the whole galaxy (top). In the age-metallicity plane (left) we plot the weights of each model to fit the ages and metallicities of the stars (red spectrum). Each white point in this plot is a model with a different age and metallicity.

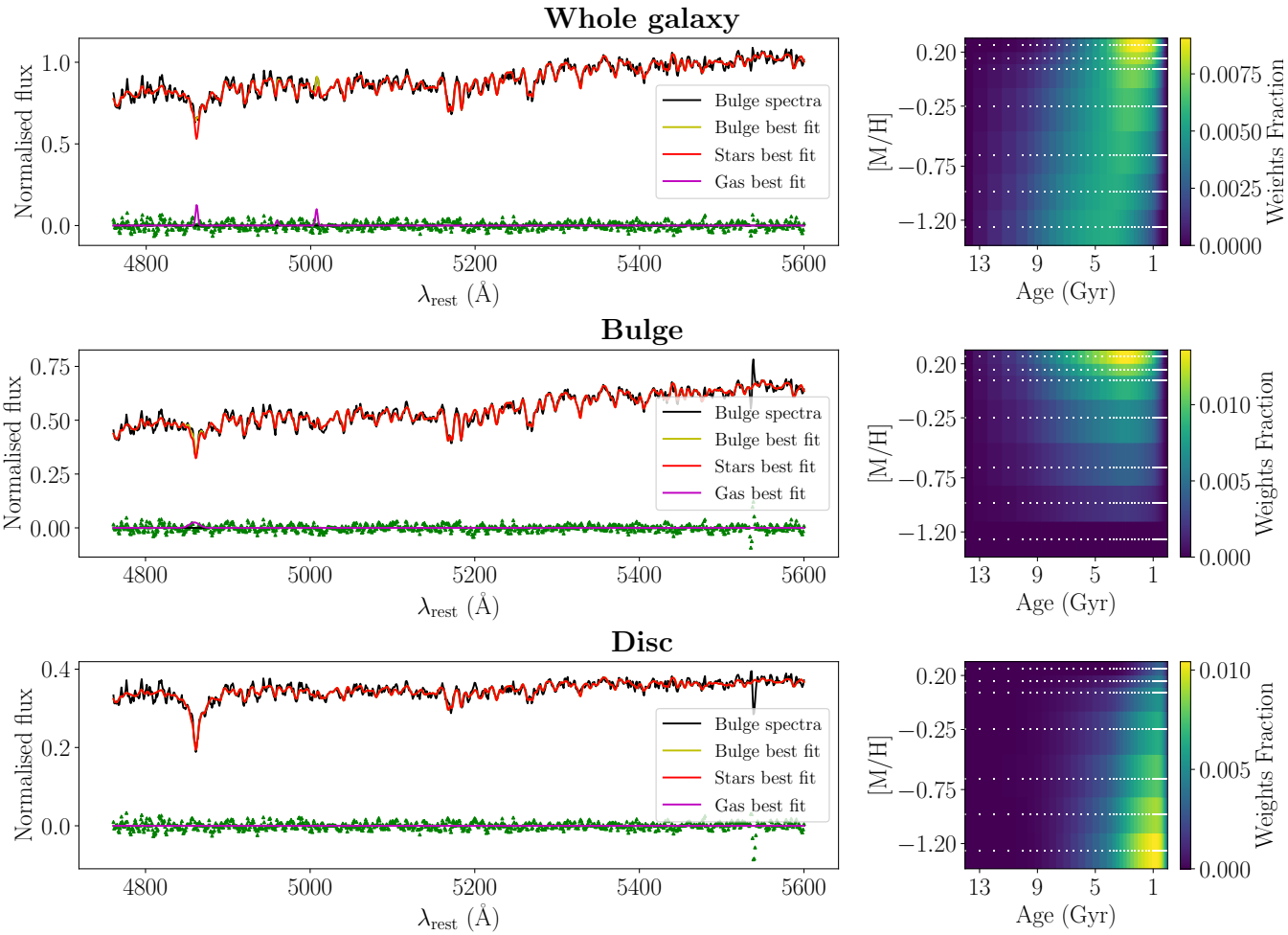

Figure A.4: Fit obtained with pPXF of the spectra (left) and age-metallicity plane (right) of central voxel of (from up tu down) the whole galaxy, the bulge and the disc of NGC7448. In the spectrum adjustment (left) we plot: the spectra of those central voxels of each datacubes (black), the best fit of pPXF with the different models for the stars (red) and for the gas (purple), the sum of both (yellow) and the residual of the fits with the spectrum (green scatter). The flux has been normalised to the value of the spectrum continuum of the whole galaxy (top). In the age-metallicity plane (left) we plot the weights of each model to fit the ages and metallicities of the stars (red spectrum). Each white point in this plot is a model with a different age and metallicity. It is important to note that the whole galaxy fit still has gas (the gas fit here is the one used to remove the gas emission) but the bulge and disc fit have no longer gas, which is why we don't see a purple line at any point.